

LC Ladder Based Orthonormal Filter for Impulse-Radio UWB Pulse Generation.

Yousif Shamsa

Supervisor: Dr. Ir. Wouter A. Serdijn

A Thesis Submitted to
The Faculty of Electrical Engineering, Mathematics and Computer
Science in Partial Fulfillment of the Requirements for the Degree of
MASTER OF SCIENCE
in Electrical Engineering

Delft University of Technology

August 2009

Abstract

Ultra Wide Band (UWB) technology is gaining momentum since 2002, when the Federal Communications Commission (FCC) approved this technology for commercial applications. UWB promises great potential for high speed communication without exclusive frequency allocation. Impulse-Radio UWB (IR-UWB) forms one of the possible candidates to implement UWB communication. IR-UWB utilizes very short pulses as information carriers, which results in a very wide band frequency spectrum. This is the reason why FCC allocated 7.5GHz of the bandwidth to UWB (3.1-10.6 GHz). One of the most challenging parts of IR-UWB transceivers is the pulse generator.

In this thesis, a UWB pulse generator is designed to be implemented in IBM 0.13 μm technology. The pulse generator has a high spectral efficiency. Using amplitude control, any mismatch, process variation or temperature variation can be compensated for to comply with the UWB FCC mask. The pulse has an approximate duration of 2ns. The current consumption is 13mA per pulse. The power consumption per pulse is 19.5 mW. The next stage can be a power amplifier or an antenna. In case of an antenna, the effect of bond pads and bond wires are taken into account.

A challenging aspect of UWB systems is their interference with narrow-band systems. Narrow-band systems send very high power signals compared to the UWB signals and thus may saturate the UWB receiver and/or prevent reliable detection of the UWB pulses. A possible solution to this problem is filtering. In this thesis, a Wireless Local Area Network (WLAN) band rejection filter for UWB applications is designed using IBM 0.13 μm technology. A new filter topology is used to implement the filter. This topology has the ability to actively read all the states of an LC filter without using extra inductors. Both AC and impulse responses are presented. The filter has a notch of approximately 14dB. It can operate over the military temperature range (-40 °C to 125 °C). The effects of mismatch and process variations on this design are acceptable.

Acknowledgement

This work would not have been possible without the support and encouragement of others. Foremost, I would like to thank my supervisor, Dr. Wouter Serdijn, for his mentorship and supervision. His inspiring lectures during the bachelor and the master years were the reason to choose micro electronics. He provided me with many helpful suggestions, important advice and constant encouragement during this work. I would like to thank Prof. John Long for giving RF IC design lectures.

I would also like to thank all the members of the Ultra-Wide Band research group and the members of DIMES in general. Yixiong Hu, Hou Rui and Saleem Al-Ahdab were a great help, but even more important, good friends whose friendship will last forever.

I would also like to thank Mohammed Reza Tajari for the help and the support throughout the bachelor and the master years. What began as a friendship ended up in a brotherhood.

Last but not least, I express my deepest appreciation to my wonderful family. My father, Dr. Salman Shamsa, my mother, Lamia El-Gerawy, my wife Lamis Chkare and my brothers Basim and Sinan were a source of inspiration and love throughout my life. To them I dedicate this work.

Contents

1	Introduction	1
1.1	Framework of the Project	1
1.2	Overview of UWB Technology	1
1.2.1	UWB Definition	2
1.2.2	UWB Regulations	3
1.2.3	UWB Applications	4
1.2.4	UWB Types	6
1.2.5	UWB Standards	6
1.3	IR (Impulse Radio)	7
1.3.1	IR Definition	7
1.3.2	IR Types	7
1.4	Problem Statement and Motivation	9
1.5	Outline of the Thesis Report	10
2	Pulse Design	11
2.1	Autocorrelation UWB System Simulation	11
2.2	Comparing UWB Pulses	14
2.3	Conclusion	16
3	Pulse Generation Principles	17
3.1	Classification of Pulse Generators	17
3.2	Static Linear Pulse Generators	18
3.2.1	Adder Based Pulse Generator	18
3.3	Static Non-Linear Pulse Generators	18
3.3.1	Multiplier Based Pulse Generator	18
3.4	Dynamic Linear Pulse Generators	20
3.4.1	Integrator Based Pulse Generator	20

3.4.2	Differentiator Based Pulse Generator	20
3.5	Dynamic Non-Linear Pulse Generators	21
3.5.1	Oscillator Based Pulse Generator	21
3.6	Conclusion	23
4	Topology Design	25
4.1	Filter Topologies	25
4.1.1	Gm-C Topology	25
4.1.2	LC Topology	26
4.1.3	Gyrator-C Topology	29
4.1.4	Conclusion	30
4.2	Transfer Function to LC Topology Translation	31
4.2.1	Transfer Function	31
4.2.2	State Space Description	33
4.2.3	Orthonormal State Space	34
4.2.4	LC filter components values	35
4.3	Conclusion	36
5	Circuit Design	37
5.1	Dirac Pulse Generator	38
5.2	LC Ladder	39
5.3	State Readout Circuit	40
5.4	Simulation Results	41
5.4.1	Simulation results in case of a power amplifier as the next stage .	43
5.4.2	Simulation results in case of an antenna as the next stage	47
5.5	Conclusion	52
6	LC Filter States Readout	53
6.1	Previous Solutions	53
6.2	Novel Solution	55
6.3	Band Rejection Filter Design	56
6.3.1	Matlab Design	56
6.3.2	Circuit Design	63
6.3.3	Conclusion	67
7	Conclusions and Future Work	69
7.1	Conclusion	69

<i>CONTENTS</i>	ix
7.2 Own Contributions	70
7.3 Future Work	70
A A discussion on antenna-LNA interface	71
A.1 Introduction to impedance match	71
A.2 Power match	72
A.3 Mismatched interface and simulation results	74
B Matlab Code	79
B.1 Matlab Code UWB Pulse Generator (Chapter 4)	79
B.2 Matlab Code Band Rejection Filter (Chapter 6)	87

List of Figures

1.1	FCC indoor effective isotropic radiated power (EIRP) limit in dBm/MHz	4
1.2	IR modulation types [1]	9
1.3	UWB-IR transmitter	9
2.1	Quadrature downconversion autocorrelation receiver (QDAR)	12
2.2	Simplified autocorrelation transceiver	12
2.3	Working UWB transceiver.	13
2.4	Input wave forms with equal power	14
2.5	Output of the system for different input wave forms.	15
2.6	Average output of the system with different input wave forms.	15
3.1	Adder based pulse generator	18
3.2	Multiplier based pulse generator	19
3.3	Relaxation oscillator based pulse generator [2]	21
3.4	Tail current and modulated gaussian pulse generated by relaxation oscillator [2]	22
4.1	Gm-C filter	26
4.2	Low Pass Based LC Realization	27
4.3	Low Pass Based LC with identical Gm blocks	28
4.4	High Pass Based LC Realization	28
4.5	Low pass gyrator-C filter	29
4.6	High pass gyrator-C filter	30
4.7	Different elliptic filter transfer functions with different orders	32
4.8	The spectral efficiency for different order approximations	32
4.9	Inductors variations for different order approximations	33
5.1	UWB pulse generator.	37

5.2	Dirac pulse generator.	38
5.3	Dirac pulse generator's output.	38
5.4	LC ladder	39
5.5	AC response of the UWB pulse generator	41
5.6	Monte Carlo analysis of AC response of the UWB pulse generator	42
5.7	Circuit implementation of the UWB pulse generator	43
5.8	AC response of the UWB pulse generator	43
5.9	AC response of the UWB pulse generator over military temperature range of operation	44
5.10	The effect of mismatch and process variation on the AC response of the UWB generator	44
5.11	UWB pulse generated by transient simulation	45
5.12	UWB pulse over military temperature range of operation	45
5.13	The effect of mismatch and process variation on the UWB pulse	46
5.14	UWB pulse amplitude control	47
5.15	AC response of the UWB pulse generator	48
5.16	AC response of the UWB pulse generator over military temperature range of operation	48
5.17	The effect of mismatch and process variation on the AC response of the UWB generator	49
5.18	UWB pulse generated by transient simulation	50
5.19	UWB pulse over military temperature range of operation	50
5.20	The effect of mismatch and process variation on the UWB pulse	51
5.21	UWB pulse amplitude control	51
6.1	Transformer-C filter [3]	54
6.2	Dual ladder filter [4]	54
6.3	Sensing the current using a resistor	55
6.4	The current through an inductor	55
6.5	A structure to read out the current in an inductor	56
6.6	A filter utilizing the structure to sense the current in an inductor	57
6.7	Magnitude bode diagram of the ideal band rejection filter design	58
6.8	Filter's states magnitude bode diagram	60
6.9	AC response of the total filter and the 4 th state of the filter	61
6.10	The 4 th state as a voltage over a capacitor	62
6.11	The 4 th state as a current through the inductor	62

6.12	Band rejection filter circuit	64
6.13	AC response of the band rejection filter	65
6.14	AC response over military temprature range of operation.	66
6.15	The effect of mismatch and process variation on the AC response	66
6.16	Impulse responce of the band rejection filter	67
A.1	Matching network for fixed source and load to maximize voltage transfer	72
A.2	(a)Inductively-degenerated LNA and (b)resonating common source LNA	73
A.3	$ S_{11} $ of the ideal monopole antenna designed for 2.4GHz	74
A.4	Receiving mode antenna setup	75
A.5	Voltage monitored on the capacitor in series with a resonating inductor and a varying resistor	75
A.6	$ S_{11} $ of a wideband antenna with receiving frequency range of 4 ~ 6GHz	76
A.7	Pulse received by 4 ~ 6GHz wideband antenna	77

List of Tables

1.1	UWB regulations in different regions of the world [5]	3
1.2	UWB regulations in the US (dBm/MHz) [5]	4
1.3	Different Technologies for IEEE 802.15.3a [6]	7
3.1	Building blocks of pulse generators	17
4.1	The number of active elements in Gm-c and gyrator based filters	29
4.2	Comparison of Gm-c, high pass gyrator-c and LC filters	30
5.1	Capacitors specifications	40
5.2	Inductors specifications	40
5.3	Performance summary	52
6.1	Capacitors specifications	63
6.2	Inductors specifications	63
6.3	Transistors specifications	65
6.4	Performance summary	68

Chapter 1

Introduction

In this introduction the framework of this research is explained and a short summary is given. First an overview of Ultra Wide Band (UWB) technology is given. Its definition, regulations, applications, types and standards are explained. Then a particular type of UWB communication, Impulse Radio (IR), is defined and categorized. After this, a problem statement and motivation are presented. Finally the outline of the thesis report is presented.

1.1 Framework of the Project

“This work is made in the framework of Ad-hoc Impulse Radio: Local Instantaneous Networks (AIR-LINK) project. The project attempts to answer the question: how can a multi-user ad-hoc network be built using UWB technology. The project members work on new hardware architectures and implementations, the physical layer with signal processing, modulation, coding and synchronization, and the link layer at which the multiple access scheme and the network architecture is defined.” [7]

1.2 Overview of UWB Technology

UWB has the potential to become the standard wireless unlicensed, short range, high speed network technology of the future. It started gaining momentum from 2002, when the Federal Communications Commission (FCC) opened the door for commercial development [8,9]. UWB systems have the following features in common:

1. The high bandwidth (7.5 GHz in the US) makes the propagation through walls and other materials possible due to the presence of low frequencies in the sent

signal.

2. The low Power Spectral Density (PSD) of the UWB signal makes coexistence between UWB and narrow-band systems possible and is the reason for the unlicensed character of the UWB.
3. The short duration of the pulses makes UWB systems immune to multipath and jamming, which makes high data rates possible (up to 1 Gbps). This feature also makes accurate positioning possible.

The importance of the bandwidth is made clear by Shannon's formula for the capacity of a single user in Additive White Gaussian Noise (AWGN) channel. From Shannon's formula shown in Equation 1.1, it is easy to see that the channel capacity (C) is proportional to the bandwidth (B) and to the logarithm of the Signal to Noise Ratio (SNR). This makes bandwidth modification an attractive approach for increasing the channel capacity. Moreover, Equation 1.1 shows that when a very large bandwidth is used, the SNR can be very low, while the system is able to realize a high channel capacity.

$$C = B \log_2(1 + \text{SNR}) \quad (1.1)$$

1.2.1 UWB Definition

FCC defines the UWB transmitter to be an intentional radiator, with either:

- an absolute bandwidth B equal to or greater than 500 MHz
- a fractional bandwidth B_f equal to or greater than 0.20

at any given moment in time. The first condition translates into Equation 1.2. The second condition is shown in Equation 1.3 and Equation 1.4, where f_h and f_l are the -10dB higher and lower frequencies.

$$B \geq 500\text{MHz} \quad (1.2)$$

$$B_f \geq 0.2 \quad (1.3)$$

$$B_f = 2 \frac{f_h - f_l}{f_h + f_l} \quad (1.4)$$

1.2.2 UWB Regulations

In each country, a regulatory body exists that regulates the use of the radio spectrum. It allocates a particular frequency to each sender and restricts the maximum of emitted power. In the beginning, the regulatory organizations resisted the creation of commercial UWB radio systems. Several concerns were raised by the Department of Defense, the Department of Transportation, the Federal Aviation Administration and Cellular and Personal Communications service companies. Finally the FCC approved the UWB after studying all the concerns. The current rules in different regions of the world are summarized in Table 1.1. Detailed information about the rules in the US is shown in Table 1.2 and Figure 1.1.

Table 1.1: UWB regulations in different regions of the world [5]

Region	Organization	Date	Frequencies
USA	FCC ¹	February 2002	3.1-10.6 GHz
Europe	CEPT/ECC ²	March 2006	3.1-4.8(until 1010) and 6-8.5 GHz
Japan	MIC ³	August 2005	3.4-4.8 and 7.25-10.25 GHz

¹Federal Communications Commission

²The European Conference of Postal and Telecommunications / Electronic Communications Committee

³Ministry of Internal Affairs and Communications

Table 1.2: UWB regulations in the US (dBm/MHz) [5]

Frequency Range (MHz)	Indoor EIRP limit	Outdoor EIRP limit	Part 15 limit
Lower than 960	-41.3	-41.3	-41.3
960-1610	-75.3	-75.3	-41.3
1610-1990	-53.3	-63.3	-41.3
1990-3100	-51.3	-61.3	-41.3
3100-10600	-41.3	-41.3	-41.3
Above 10600	-51.3	-61.3	-41.3

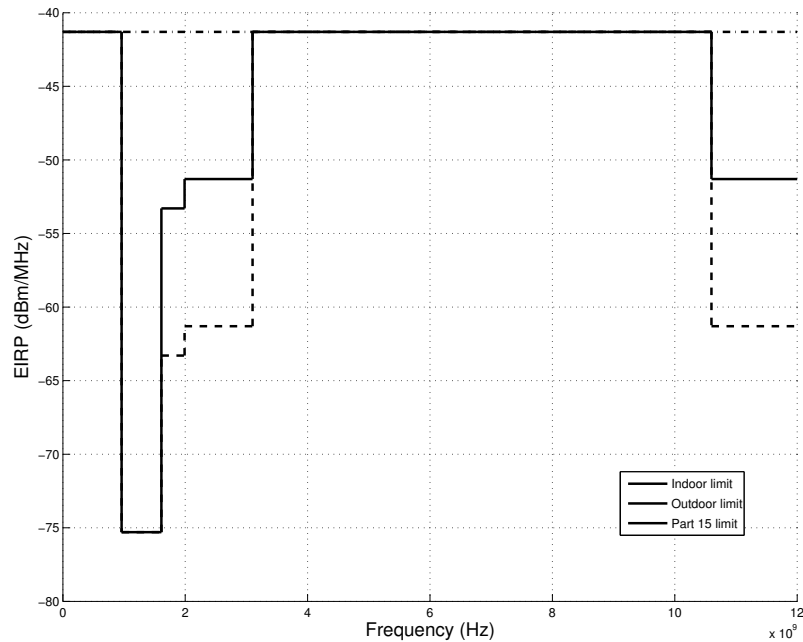


Figure 1.1: FCC indoor effective isotropic radiated power (EIRP) limit in dBm/MHz

1.2.3 UWB Applications

UWB communication has a broad range of applications which are summarized as follows:

1. Communication

- (a) High speed communication:
- i. Connectivity between a host and associated peripherals
 - ii. Streaming of digital media content between consumer electronic devices (TV, VCR, CD/DVD players, mp3 players)
 - iii. The short duration of the pulses and its low power density makes the signal appear to other radio systems as noise. UWB is also immune to interference from other radio systems. These properties makes UWB suitable for military communication.
- (b) Low speed communication: The most important application in this category is sensor networks. A sensor network has the possibility of low to medium rate and large range communication with positioning capability. The IEEE 802.15.4a standard is specialized in this category of applications.

2. **Imaging** The second application group of UWB is imaging. The early utilization of UWB technology were primarily radar related, because of the high penetration ability of the low frequencies. Another reason for using UWB in radar applications is the fine range resolution that comes with large bandwidth [10]. The current applications are:

- Through-wall imaging: can provide health and location monitoring of fire-fighters or hostages.
- Ground-penetrating radar: It is widely used for both military as for civilian purposes. Land mine detection, concrete inspection and bridge deck evaluation are some examples of the use of GPR.
- Medical imaging: UWB is used in the medical world because of its capability of diagnosis of breast cancer. It also allows non-invasive monitoring applications of human vital signs such as respiration and heart rates. Other applications are: multi-patient monitoring and detection of cardiac arrhythmia.

3. **Position location and tracking** UWB can be used as an indoor positioning system.

- The system can be used by firemen to locate themselves and track team members.
- It can also be used for surveillance. The system detects and tracks movements of non-authorized personnel, craft, robots, and vehicles crossing perimeters and entering secure areas.

1.2.4 UWB Types

UWB radios can be divided into two groups based on the use of the UWB bandwidth. The technology utilizing pulses which occupies the entire allowed frequency range is called Impulse Radio Ultra Wide Band (IR-UWB). The other type of UWB radio is Multi-Band Orthogonal Frequency Division Multiplexing Ultra Wide Band (MB-OFDM UWB), which divides the allowed bandwidth into 14 bands, each 500 MHz wide.

IR-UWB uses ultra short pulses which occupy the entire allowed frequency band (3.1-10.6 GHz in the US). The advantages of IR compared to OFDM are:

1. It has the potential for low cost, low complexity transceivers because no Fourier transformations are needed like in the case of OFDM.
2. It has positioning possibility while OFDM-UWB does not.
3. It has lower probability of interception/detection (LPI/LPD).

On the other hand, OFDM-UWB uses multiple orthogonal carriers. Each carrier is modulated separately and finally all the carriers are added to construct the total signal. The main advantage of OFDM compared to IR is the flexibility of the devices to adjust to the regulations and to channel conditions by using or avoiding using a band or multiple bands.

1.2.5 UWB Standards

There are different standardization groups in the UWB world. Most important groups are mentioned and discussed in this section.

IEEE 802.15.3a (WPAN High Rate Alternative PHY) This group attempted to make a global standard for the high speed UWB. The group withdrew itself in 2006 because the two alliances, the UWB Forum (IR UWB) and WiMedia Alliance (MB-OFDM UWB), could not reach an agreement on the standard. In Table 1.3 a comparison between different technologies is seen for high rate UWB communication systems.

IEEE 802.15.4a (WPAN Low Rate Alternative PHY) This group targets: providing communications and high precision location capability (1 meter accuracy and better), high aggregate throughput, and ultra low power as well as adding scala-

Table 1.3: Different Technologies for IEEE 802.15.3a [6]

Name	Wireless USB	Cable free	Certified Wireless USB
Technology	UWB-IR	UWB-IR	OFDM
Organization	UWB Forum	No	WiMedia Alliance
Leading Company	Pulse Link	Freescale	Intel
MA Used	Direct-Sequence UWB	Direct-Sequence UWB	OFDM
Max. Data Rate	1.35 Gbits/sec	110 Mbits/sec	480 Mbits/sec
Max transmission range	3 m	10 m	10 m

bility to data rates, longer range, and lower power consumption and cost. One of the applications for this standard is a wireless sensor network.

1.3 IR (Impulse Radio)

In this section UWB impulse radio is defined and different types of impulse radios are categorized.

1.3.1 IR Definition

UWB Impulse radio is defined as a radio system which uses ultra short pulses in the time domain to communicate. The short transient pulses occupy the entire allowed frequency band (3.1-10.6 GHz in the US).

1.3.2 IR Types

The impulse radios can be categorized based on: receiver's structure, multiple access scheme and modulation type.

Types of impulse radios based on receiver structure: Based on the structure IRs can be divided in coherent and non-coherent receivers. Auto-correlation (AC) receivers, Transmitted-reference (TR) and Energy detection receivers are different types of non-coherent receivers.

Types of impulse radios based on the multiple access: Multiple access refers to techniques that enable multiple users to share the available bandwidth [11].

1. Direct Sequence (DS): a spread spectrum modulation technique and a way to accomplish multiple access. It works by multiplying the data with a pseudo-random code. The code is composed of a pseudo-random sequence of 1 and -1 at a much higher frequency than the original signal. The sequence is known for both the transmitter and the receiver. At the receiver side the data is multiplied again with the same sequence. This will reconstruct the original data. This process of gaining the original data is called de-spreading. If an undesired transmitter transmits on the same channel but with a different sequence (or no sequence at all), the signal will be seen as noise. This is how the multiple access is accomplished [12].
2. Time Hopping (TH): a spread spectrum modulation technique and a way to accomplish multiple access. It works by sending extremely short pulses at random or pseudo-random time instants using a sequence called TH code. Each receiver has its own TH code. Based on this code it is possible to determine the destination receiver. If the TH code of multiple transceiver pairs differs enough from each other it is possible to accomplish multiple access [13, 14].

Types of impulse radios based on modulation: In the transmission of digital information over a communication channel, the digital information has to be converted to analog waveforms. This conversion is called modulation [5]. Different modulation techniques are depicted in Figure 1.2.

1. PPM (Pulse Position Modulation): the information is in the position of the pulse. It has discrete spectral lines in the power spectral density (PSD). This results in low spectral efficiency.
2. PAM(Pulse Amplitude Modulation): the information is in the amplitude of the pulse. It has a smooth PSD what forms a great advantage comparing to the other two modulation techniques because the high spectral efficiency. The smooth PSD is a result of the random polarities of the information symbols [1].
3. OOK(On Off Keying): the information is in the presence or absence of the pulse. It has a discrete spectral lines in the PSD. The advantage of OOK compared to the other two is the receiver reduced complexity.

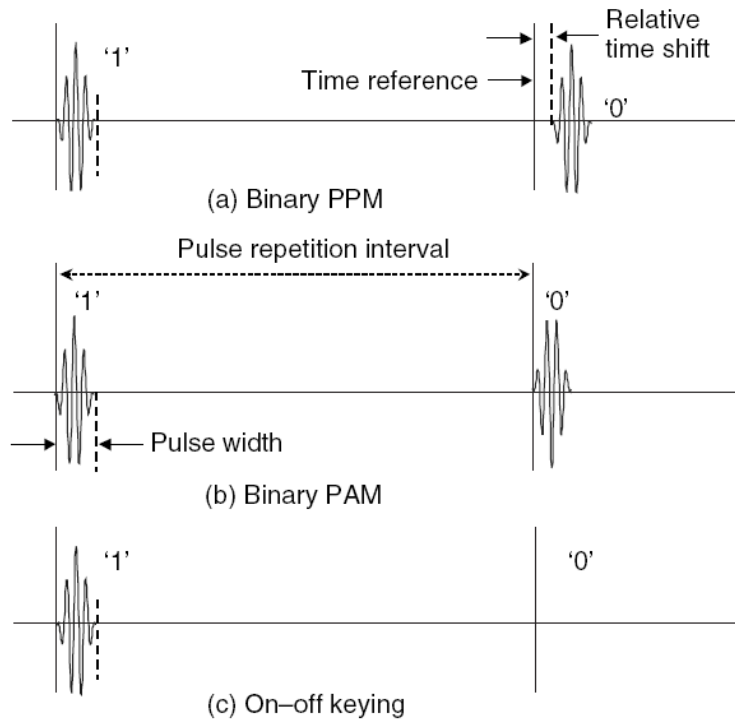


Figure 1.2: IR modulation types [1]

1.4 Problem Statement and Motivation

An IR transmitter exists of a digital part (DS), a digital to analog converter (DAC), a pulse modulator (PM), a pulse generator (PG), a power amplifier (PA) and an antenna, shown in Figure 1.3 A low voltage, low power, integrated UWB pulse generator is designed in IBM $0.13\mu\text{m}$ CMOS technology. The design challenges are the power consumption and the spectral efficiency. The performance of the pulse generator should be comparable to the state of art. Also the interface between the power amplifier and the antenna and between the antenna and the low noise amplifier (LNA) is studied.

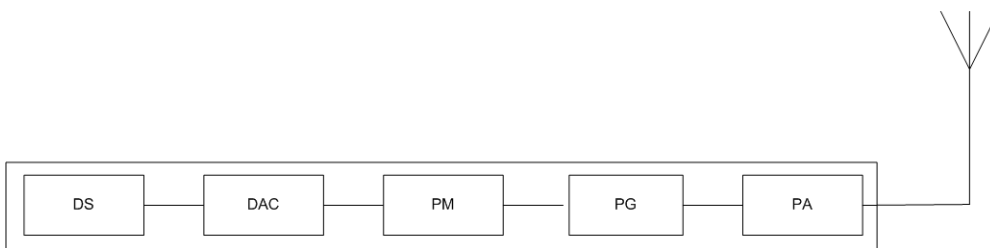


Figure 1.3: UWB-IR transmitter

1.5 Outline of the Thesis Report

This thesis is organized as follows. Chapter 2 covers pulse design. In Chapter 3 the pulse generation principles are studied. The topology of the pulse generator is selected in Chapter 4. Finally the circuit design is done in Chapter 5. In Chapter 6 a new filter topology is studied and a band rejection filter is designed. In Appendix A a broadband antenna is designed and characterized. Then the necessity of impedance matching between the antenna and the next (LNA) or previous (Pulse generator or Power amplifier) circuits is studied.

Chapter 2

Pulse Design

IR UWB technology utilizes short pulses for wireless communication. The pulses have to comply to the FCC effective isotropic radiated power (EIRP) while transmitting the highest power possible. In Section 2.1 a UWB system simulator is build using Matlab. Then in Section 2.2 the simulator is tested with different signals. In Section 2.3 test results are presented.

2.1 Autocorrelation UWB System Simulation

In the Autocorrelation UWB Transceiver pulses are transmitted with a predefined delay τ . The first pulse acts as a reference, whereas the second pulse is modulated in polarity. The autocorrelation receiver correlates the reference pulse with the modulated pulse. The absolute value of the output after integration is in fact the energy of the pulse while the polarity of the output contains the data [15]. This technique makes synchronization with the individual pulses unnecessary. It also combines the energy from multipath reflections at the receiver, enhancing the received Signal to Noise Ratio (SNR) [16]. In Figure 2.1 an autocorrelation receiver is depicted.

To simulate the receiver, some simplifications have to be made. A simplified transceiver topology is depicted in Figure 2.2. Both receiving and sending antennas response is assumed to be flat. The channel is assumed to be an Additive Gaussian White Noise (AGWN) channel. Using Matlab, the gaussian white noise is added to the signal. LNA and the filter are not important in the choice of the pulse so these parts are also ignored. The important part of the correlation receiver is the delay and the multiplier combination. The delay element ensures that the current pulse is multiplied with the previous pulse. Three components will results from this multiplication: $s \cdot s$,

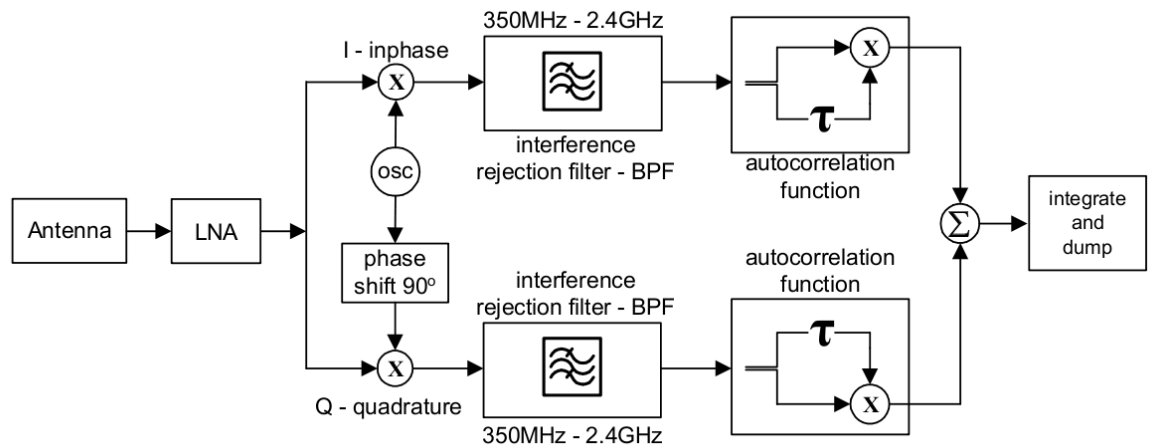


Figure 2.1: Quadrature downconversion autocorrelation receiver (QDAR)

$s \cdot n$ and $n \cdot n$. The multiplication and the integration of the result will cause filtering of the noise because average squared value of the second and the third term ($s \cdot n$ and $n \cdot n$) is zero while average squared value of the first term ($s \cdot s$) is positive (in case both pulses are in phase). This part is simulated by adding noise to the send signals and multiplying the sent signal with a delayed version of it self. In Figure 2.3 the working of autocorrelation receiver is shown.

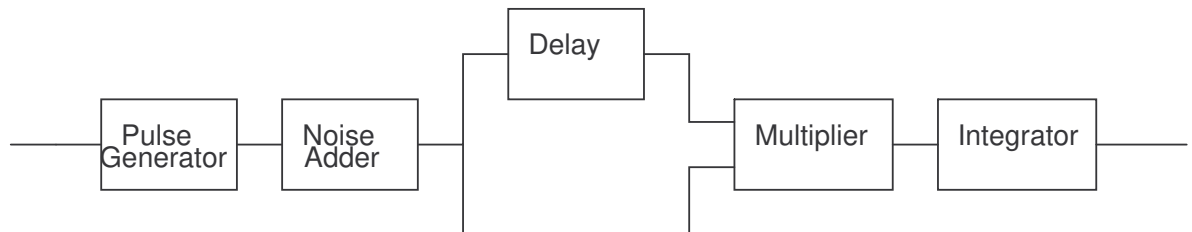


Figure 2.2: Simplified autocorrelation transceiver

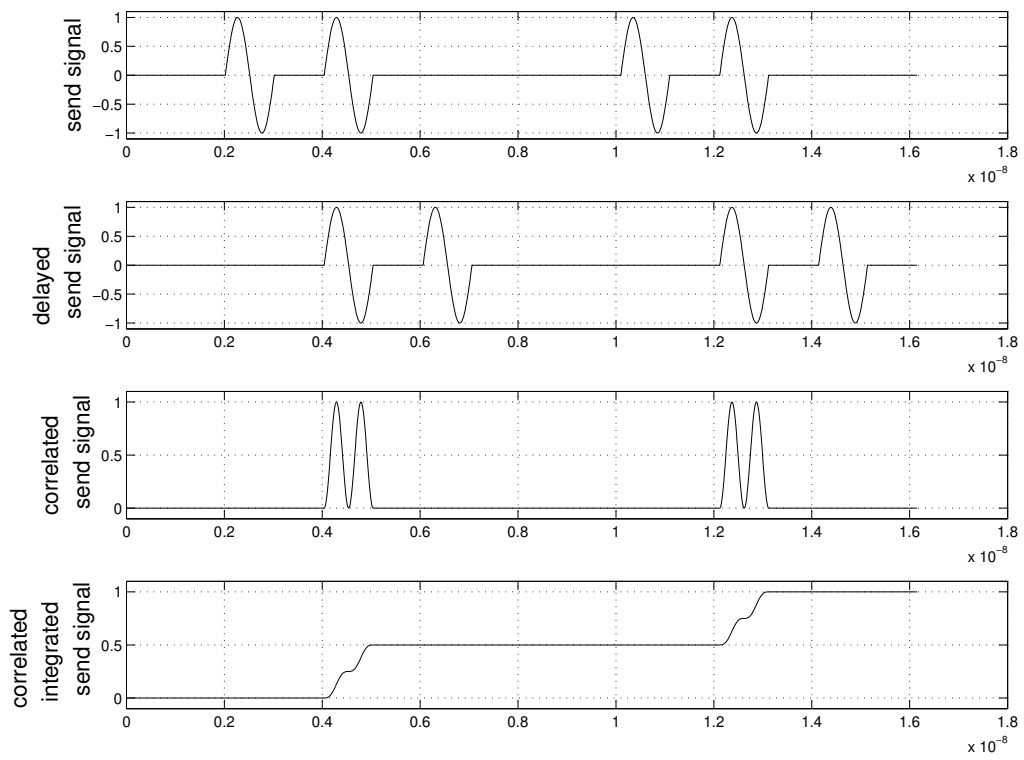


Figure 2.3: Working UWB transceiver.

2.2 Comparing UWB Pulses

Two aspects of the pulses are tested, the power content of the pulses and the pulse shape. This is done by using two signals with constant power content and different pulse shapes as entry for the transceiver. The input signals are depicted in Figure 2.4. The channel adds noise to the signals. The receiver delays the signal and correlates it with the non-delayed signal. Finally the receiver integrates the signal. This causes filtering of the noise which will have a mean value equal to zero. In Figure 2.5 the output of the system in both cases is seen. The noise is a random factor so it will differ each time the system is simulated. To eliminate this factor the system is simulated a couple of times and the results are being averaged. The result is seen in Figure 2.6. In this figure the mean final value versus number of simulations is depicted. It is clear that both input signals produce on average the same output. From this it can be concluded that the power content of the signal determines the received signal independently of the wave form.

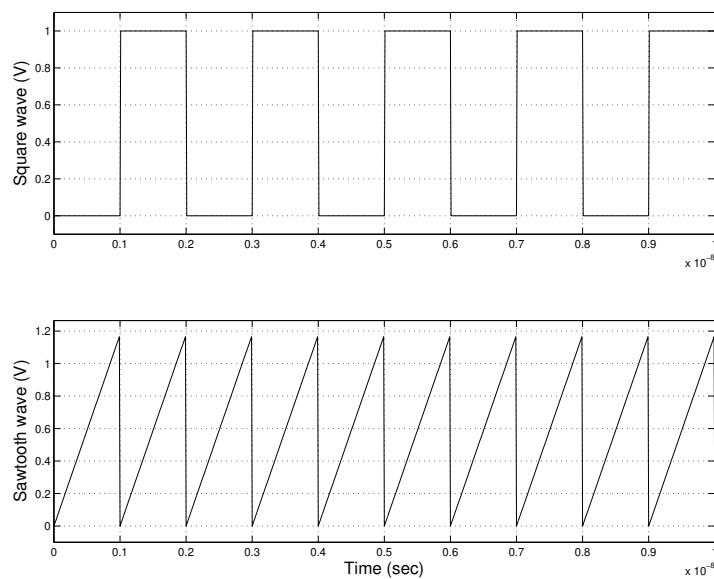


Figure 2.4: Input wave forms with equal power

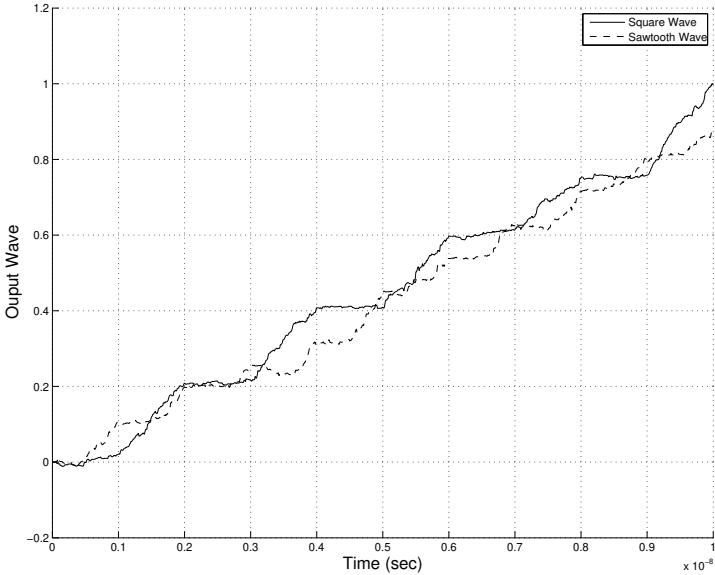


Figure 2.5: Output of the system for different input wave forms.

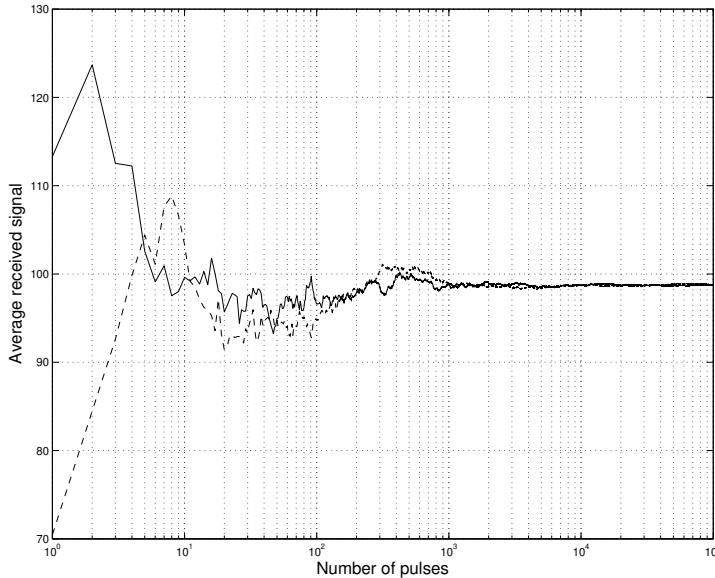


Figure 2.6: Average output of the system with different input wave forms.

2.3 Conclusion

In an autocorrelation receiver, the power content of the signal and not the shape of the pulse determines the SNR of the received signal. For the UWB pulse, the highest possible power is achieved when the pulse in the frequency domain has the same shape as the UWB FCC mask. In that case the spectral efficiency equals 100%. The frequency spectrum has to be translated to a transfer function in order to implement it using an electronic circuit.

Chapter 3

Pulse Generation Principles

Many articles are published about UWB pulse generators up to now. Yet a lot of them share the same fundamental ways of operating. In this section, these fundamental principles of pulse generation is presented and categorized. First, in Section 3.1 the categorization is done. Then in Sections 3.2, 3.3, 3.4 and 3.5 different categories pulse generators are studied. Finally in Section 3.6 a conclusion is presented.

3.1 Classification of Pulse Generators

Many UWB pulse generators share the operating principle. Puls generators are categorized in this section. The categorization is done by deviding each type of pulse generators to its fundamental blocks. Examples of pulse generators are adder based, oscillator based, filter based. Examples of the fundamental blocks are seen in Table 3.1. These blocks belong to a certain principle, (static-linear, static-non-linear, dynamic-linear or dynamic-non-linear). Depending on the used blocks, the generator belongs to a certain class of the pulse generators. Next, all the principles are studied.

Table 3.1: Building blocks of pulse generators

	Static	Dynamic
Linear	Amplifier, Attenuator, Adder	Integrator, Differentiator, Delay element
Non-linear	Multiplier, tanh generator, Limiter, Switch	Oscillator

3.2 Static Linear Pulse Generators

An example of this type of generators is an adder based generators.

3.2.1 Adder Based Pulse Generator

Pulse combination method works with two successive functions. One is to generate the pulses and the other to combine them at the output stage [17]. There are a couple of possibilities for the first function. The combined pulses are mostly gaussian like pulses [17] but it is also possible to use hyperbolic tangent (tanh) pulses [18] or a monocycle sinusoid pulses [19]. An adder is used to implement the second function (combining the pulses). In Figure 3.1 a simplified scheme of an adder based pulse generator is depicted.

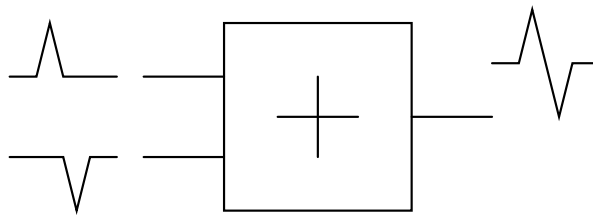


Figure 3.1: Adder based pulse generator

3.3 Static Non-Linear Pulse Generators

A multiplier, tanh generator and a limiter are some elements of the static non-linear category. The multiplier based generator is studied here.

3.3.1 Multiplier Based Pulse Generator

This generator uses pulse combination method. The difference with adder based generator is that the pulses at the input are multiplied instead of added [20]. In Figure

3.2 a simplified topology of the multiplier based pulse generator is depicted.

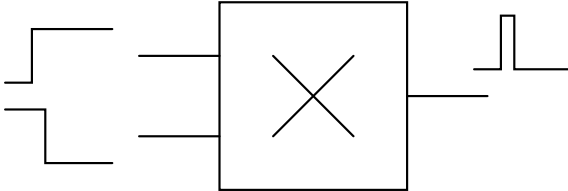


Figure 3.2: Multiplier based pulse generator

3.4 Dynamic Linear Pulse Generators

This category consists of an integrator, a differentiator and delay element.

3.4.1 Integrator Based Pulse Generator

In this type of pulse generators the pulse/step response of the system is used as an UWB pulse. The system is build by translating the transfer function of the system to a state space [21]. See Equations 3.1 and 3.2 for a general example of a state space.

$$s\mathbf{x} = [A]\mathbf{x} + [B]u \quad (3.1)$$

$$y = [C]\mathbf{x} + [D]u \quad (3.2)$$

A third order state space description is seen in Equations 3.3 and 3.4. It can be seen that each state is the integration of the weighted sum of all the states.

$$s \begin{bmatrix} x_1 \\ x_2 \\ x_3 \end{bmatrix} = \begin{bmatrix} a_{11} & a_{12} & a_{13} \\ a_{21} & a_{22} & a_{23} \\ a_{31} & a_{32} & a_{33} \end{bmatrix} \begin{bmatrix} x_1 \\ x_2 \\ x_3 \end{bmatrix} + \begin{bmatrix} b_1 \\ b_2 \\ b_3 \end{bmatrix} u \quad (3.3)$$

$$y = \begin{bmatrix} c_1 & c_2 & c_3 \end{bmatrix} \begin{bmatrix} x_1 \\ x_2 \\ x_3 \end{bmatrix} + [d]u \quad (3.4)$$

The transfer function has to approximate the FCC mask as well as possible. The FCC mask has a form of a bandpass filter, so from now on this generator is called filter based pulse generator.

3.4.2 Differentiator Based Pulse Generator

The equations 3.1 and 3.2 can be translated to the differentiator form seen in 3.5 and 3.6. To implement the new equations differentiators are needed instead of integrators. Both equation sets implement the same transfer function so also this pulse generator is called filter based.

$$\left(\frac{1}{s}\right) \dot{\mathbf{x}} = [\dot{A}]\dot{\mathbf{x}} + [\dot{B}]u \quad (3.5)$$

$$y = [\dot{C}]\dot{\mathbf{x}} + [\dot{D}]u \quad (3.6)$$

3.5 Dynamic Non-Linear Pulse Generators

In this section an oscillator based pulse generator is studied.

3.5.1 Oscillator Based Pulse Generator

An LC oscillator can be used to generate UWB pulses. The pulses are generated by modulating the tail current of a well known negative impedance LC oscillator optimized for low power consumption [22, 23].

In [2], the authors propose a relaxation oscillator to produce a modulated gaussian pulse. Again the oscillator does not generate the pulse it only bring the pulse applied to the tail current into higher frequencies. The schematics and the pulse shape are shown in Figures 3.3 and 3.4, respectively. The advantage of the relaxation oscillator above the LC oscillator, that no inductors and varactors are needed, which are greedy in integrated circuit area, and usually require a process with RF options.

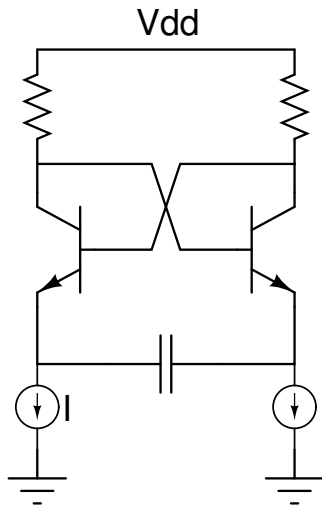


Figure 3.3: Relaxation oscillator based pulse generator [2]

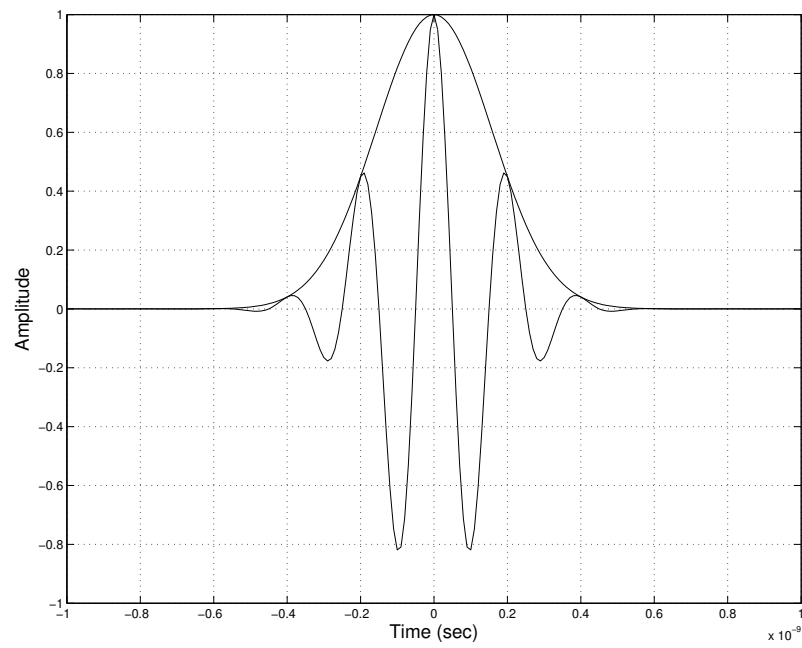


Figure 3.4: Tail current and modulated gaussian pulse generated by relaxation oscillator [2]

3.6 Conclusion

In this chapter different possibilities were discussed to generate the UWB pulse selected in Chapter 2. Among different topologies, the filter based topology will be used to implement the pulse generator. This choice is made based on the experience and the expertise with this kind of topologies in our group.

Chapter 4

Topology Design

A filter based pulse generator is a filter with a particular transfer function driven by an impulse or a step. The goal of an UWB pulse generator is to generate pulses that comply with the FCC mask with the highest spectral efficiency possible. So the magnitude transfer in the pass band to be flat and the edges of the bandpass have to be steep. At the same time the order of the filter has to be as low as possible. In Section 4.1 different filter topologies are presented. In Section 4.2 the transfer function is translated to state space description. Then the state space is translated to orthonormal state space. From the orthonormal description, components values for the LC topology are calculated.

4.1 Filter Topologies

In this section a number of topologies to realize a state space based filter will be studied. These topologies are Gm-C, LC and gyrator-C filters. The gyrator-C filter is a novel topology which has certain advantages compared to the other two filters.

4.1.1 Gm-C Topology

A Gm-C filter translates the state space description directly to a circuit form. As seen in Chapter 3, the state space description of the system consists of coefficients to implement the A, B, C and D matrices, and of integrators to calculate the next states. See Equations 3.1 and 3.2. In a Gm-C topology the capacitors implement the integrators. The Gm blocks realize the non-zero elements of the state space matrices. The states (\underline{x}) are the voltages over the capacitors. The Gm blocks representing the A matrix convert the states (voltages) to currents and multiply them with a factor. Then

the states are added and integrated using the capacitors. The Gm blocks representing the C matrix convert the states (voltages) into currents and multiply it with a factor. These currents are added to form the output. The Gm blocks implementing the A matrix have to be more accurate than the ones implementing the C matrix. The reason behind this, is that any variation of the elements of the A-matrix will cause an avalanche of variations throughout the whole filter. While any variations in the C-matrix will only lead to variations of the read out of the state.

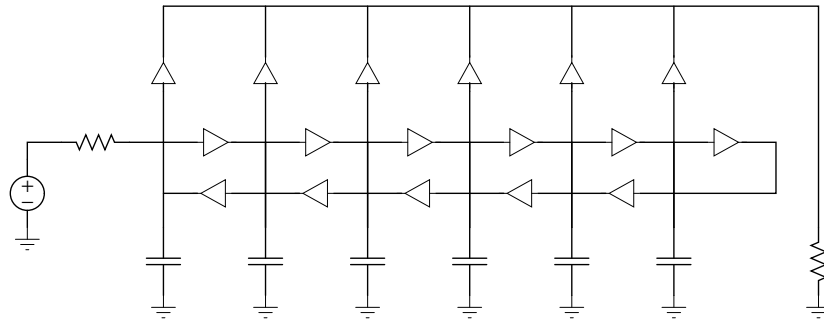


Figure 4.1: Gm-C filter

The problem of the Gm-C filter as a pulse generator is the need for extremely high bandwidth (3.1-10.6 GHz) and accurate transfer of the Gm blocks. It is also obvious that each Gm block has a different value, so each block has to be designed separately. This forms an other disadvantage of the Gm-C filter.

4.1.2 LC Topology

An orthonormal state space description can be translated directly into an LC filter. In this section two types LC filters are discussed: Low pass LC and high pass LC topology.

Low Pass LC Topology

The integrator based orthonormal state space, seen in Equations 4.1 and 4.2, can be translated into a low pass LC filter. Both the inductors and the capacitors work as integrators. They integrate the previous and the next state and produce the current state. In case of capacitance the sum of the currents is integrated into a voltage and in

case of inductors the sum of the voltages is integrated into a current. No active parts are involved in the states determination which forms a major advantage compared to the Gm-c filter. The active part is only used to calculate a weighted sum of the states, which forms the output. An important property of bandpass filters is that the elements of C-matrix are non-zero only on even or odd positions, as can be seen in Figure 4.2. This property allows us reading the voltage states only. This property simplifies the design enormously.

$$s\underline{x} = [A]\underline{x} + [B]\underline{u} \quad (4.1)$$

$$y = [C]\underline{x} + [D]\underline{u} \quad (4.2)$$

The values of the inductors and the capacitors have to be derived out of the orthonormal state space description. After that the values of inductors and capacitors have to be scaled to get acceptable values.

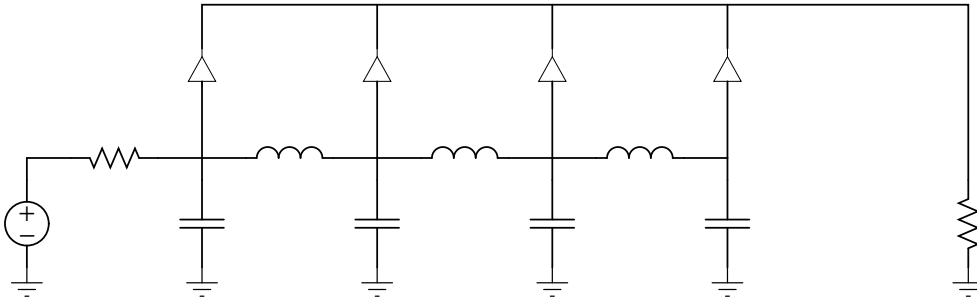


Figure 4.2: Low Pass Based LC Realization

Each Gm block in Figure 4.2 has a different value. This property complexes the design of this topology. To simplify the design the factors can be made by splitting the capacitors and using identical Gm blocks. The new topology is depicted in Figure 4.3.

High Pass LC Topology

A High Pass LC Topology implements the differentiator based state space as seen in Equations 4.3 and 4.4. Both inductors and capacitors differentiate the sum of the state before and after the current state. The topology of this filter is depicted in Figure 4.4.

$$\begin{pmatrix} 1 \\ s \end{pmatrix} \underline{x} = [A]\underline{x} + [B]\underline{u} \quad (4.3)$$

$$y = [C]\underline{x} + [D]\underline{u} \quad (4.4)$$

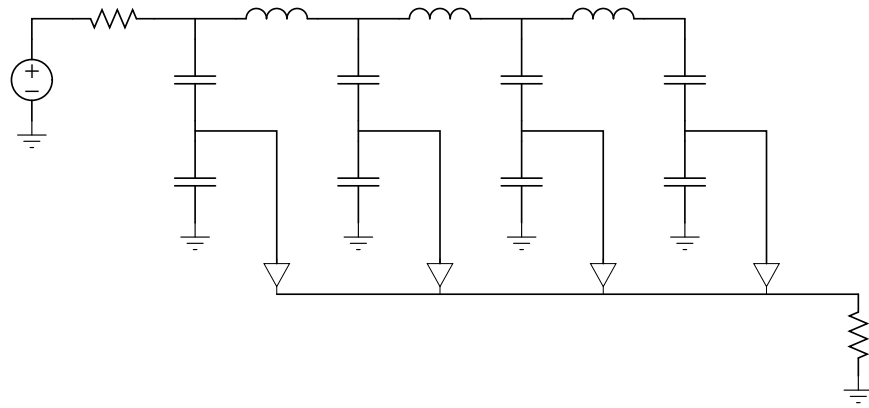


Figure 4.3: Low Pass Based LC with identical Gm blocks

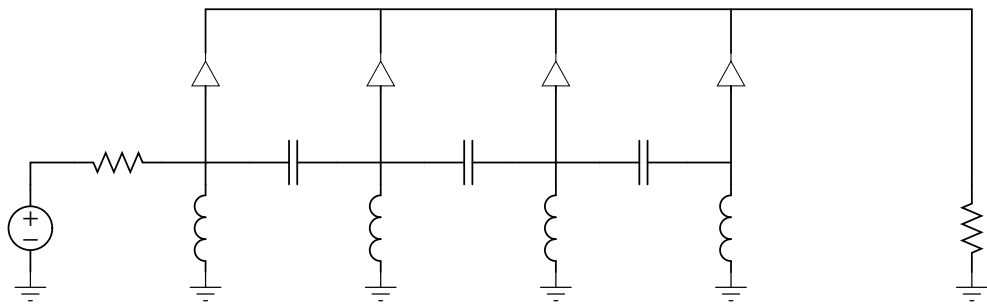


Figure 4.4: High Pass Based LC Realization

4.1.3 Gyrator-C Topology

The main problem with both low and high pass LC filters is the use of inductors. This causes chip area dissipation. A novel topology called Gyrator-C is introduced in this section. It forms a variation of the LC topologies where the inductor behavior is simulated using a gyrator and a capacitance. There are two possibilities: a low pass gyrator-C filter as seen in Figure 4.5, and a high pass gyrator-C filter seen in Figure 4.6. In table 4.1 the number of active elements for gyrator-c and Gm-c filters is summarized. The n represents the order of the system and $\#([C])$ represents the number of non-zero elements in the C matrix. From this table it is clear that a high pass gyrator-C topology has a lower number of active elements (compared to the other two topologies) and it does not suffer from area dissipation like the LC topologies.

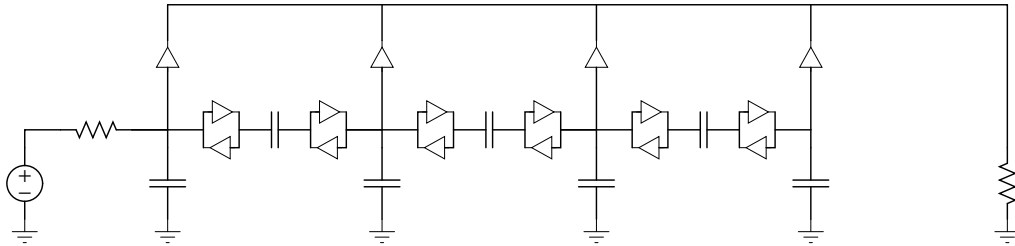


Figure 4.5: Low pass gyrator-C filter

Table 4.1: The number of active elements in Gm-c and gyrator based filters

Filter Topology	Number of active elements
Gm-C	$2n - 1 + \#([C])$
Low pass gyrator-C	$2n + \#([C])$
High pass gyrator-C	$n + \#([C])$

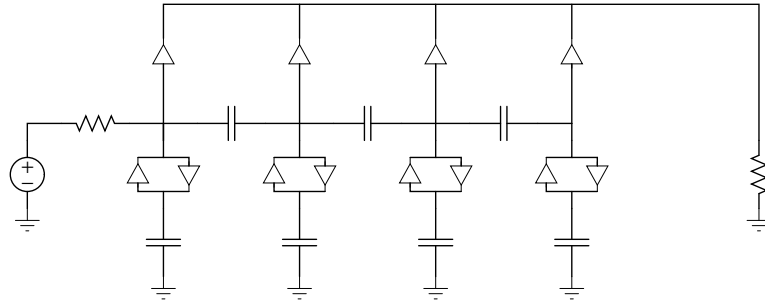


Figure 4.6: High pass gyrator-C filter

4.1.4 Conclusion

In this section three topologies were studied: Gm-C, LC and gyrator-C topologies. To make a conclusion about these topologies Table 4.2 is used. From the table we can conclude that the high pass gyrator-C filter forms a good trade off between the power and the area consumption. The LC topology is very attractive from the power consumption standpoint. From the two possibilities of LC filters the low pass topology is favored because of the lower Q-factor of grounded inductors. Since the power consumption forms a more important issue compared to area consumption, in this thesis a low pass LC filter topology is chosen to be designed.

Table 4.2: Comparison of Gm-c, high pass gyrator-c and LC filters

Filter Topology	Power consumption	Area consumption
Gm-C	-	0
High pass gyrator-C	0	0
LC	+	-

4.2 Transfer Function to LC Topology Translation

First an approximation of the FCC mask is made using an elliptic filter. Elliptic filter is used because it has a fast transition between the passband and the stopband. To implement a transfer function using the LC topology, it has to be translated to orthonormal state space. After that the transfer function of the filter is translated to an integrator based orthonormal state space. Finally the state space is translated to LC values.

4.2.1 Transfer Function

The transfer function is generated using an elliptic filter as discussed before. In Figure 4.7 different elliptic filter transfer functions with different orders are seen. The order of the filter affect the spectral efficiency and components variations. The spectral efficiency is defined as the integration of the transfer function in the 3.1 GHz to 10.6 GHz region. The spectral efficiency is proportional to the order, as seen in Figure 4.8. Components variations are inversely proportional to the order as seen in Figure 4.9. The 8th and the 10th order have a too large inductor variations which makes on chip implementation cumbersome. The 6th order forms a good trade off between the spectral efficiency and components variation. The 6th order transfer function is seen in Equation 4.5.

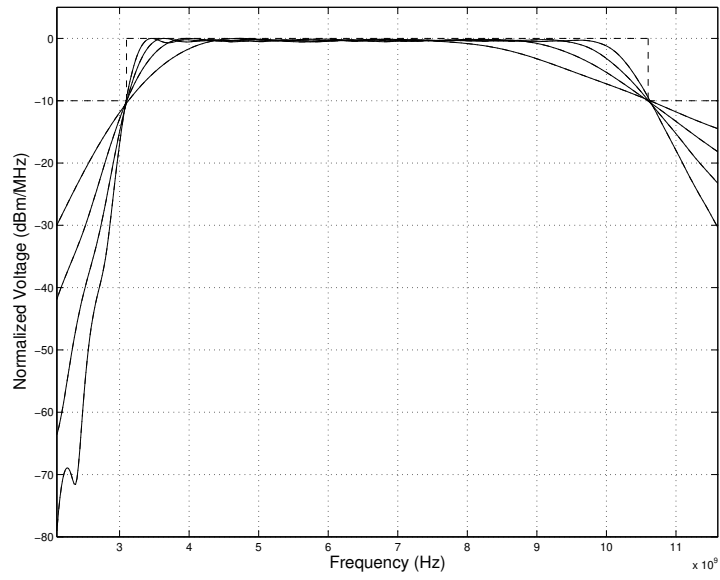


Figure 4.7: Different elliptic filter transfer functions with different orders

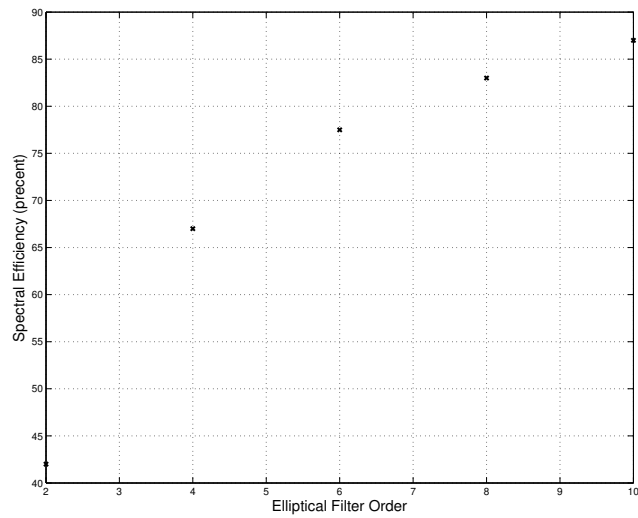


Figure 4.8: The spectral efficiency for different order approximations

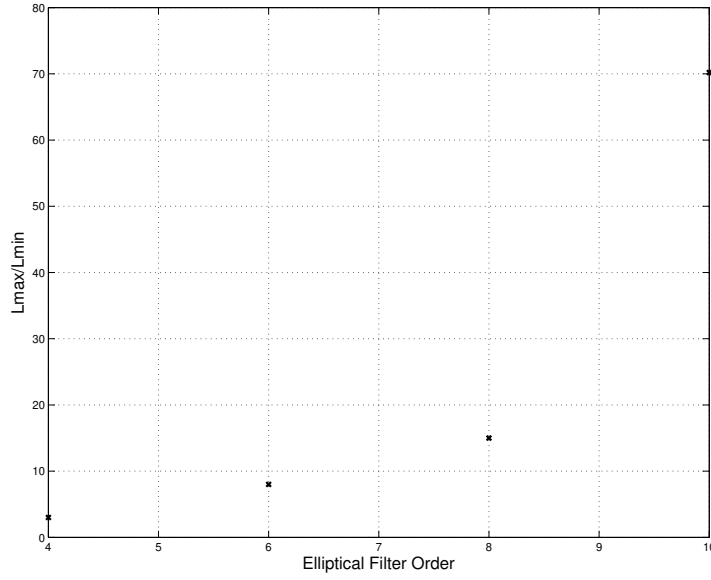


Figure 4.9: Inductors variations for different order approximations

$$H(s) = \frac{8.975e7 s^5 + 2.065e5 s^4 + 1.1e31 s^3 + 1.255e26 s^2 + 2.086e50 s - 1.912e40}{s^6 + 3.623e10 s^5 + 5.493e21 s^4 + 1.212e32 s^3 + 8.374e42 s^2 + 8.422e52 s + 3.544e63} \quad (4.5)$$

4.2.2 State Space Description

The transfer function is converted to state space. This is done using a standard command in Matlab. The state space is a not unique description of the transfer function. This makes it possible to optimize the state space as will be seen in the next section. The A, B, C and D matrices of the state space are listed in Equations 4.6, 4.7, 4.8 en 4.9.

$$A = \begin{bmatrix} -3.62e10 & -5.49e21 & -1.21e32 & -8.37e42 & -8.42e52 & -3.54e63 \\ 1 & 0 & 0 & 0 & 0 & 0 \\ 0 & 1 & 0 & 0 & 0 & 0 \\ 0 & 0 & 1 & 0 & 0 & 0 \\ 0 & 0 & 0 & 1 & 0 & 0 \\ 0 & 0 & 0 & 0 & 1 & 0 \end{bmatrix} \quad (4.6)$$

$$B = \begin{bmatrix} 1 \\ 0 \\ 0 \\ 0 \\ 0 \\ 0 \end{bmatrix} \quad (4.7)$$

$$C = \begin{bmatrix} 8.98e7 & 2.06e5 & 1.1e31 & 1.25e26 & 2.09e50 & -1.91e40 \end{bmatrix} \quad (4.8)$$

$$D = [0] \quad (4.9)$$

4.2.3 Orthonormal State Space

The state space obtained in the previous section is translated into an orthonormal state space. This form has a lot of advantages above the previous one. The number of non-zero elements in the A matrix is small. This makes it easier to implement. The dynamic range is close to the maximum. The effect of elements variations is very small [24, 25]. Another advantage is that it is possible to realize this filter using inductors and capacitors. The orthonormal state space description is listed in Equations 4.10, 4.11, 4.12 and 4.13.

$$A = \begin{bmatrix} 0 & 32.7e9 & 0 & 0 & 0 & 0 \\ -32.7e9 & 0 & 14.3e9 & 0 & 0 & 0 \\ 0 & -14.3e9 & 0 & 39.2e9 & 0 & 0 \\ 0 & 0 & -39.2e9 & 0 & 23e9 & 0 \\ 0 & 0 & 0 & -23e9 & 0 & 46.3e9 \\ 0 & 0 & 0 & 0 & -46.3e9 & -36.2e9 \end{bmatrix} \quad (4.10)$$

$$B = \begin{bmatrix} 0 \\ 0 \\ 0 \\ 0 \\ 0 \\ 1.07e05 \end{bmatrix} \quad (4.11)$$

$$C = \begin{bmatrix} 1.21e-10 & -2.12e5 & -1.11e-10 & 9.36e4 & 3.62e-11 & 836 \end{bmatrix} \quad (4.12)$$

$$D = [0] \quad (4.13)$$

4.2.4 LC filter components values

Using Matlab, the state space is translated into L, C and R values. These values are shown in Equations 4.14, 4.15 and 4.16. The values are not unique which means that it is possible to scale all the values by multiplying the L values and the R value and deviding the C values by the same factor. The scaling factor is chosen to minimize inductors size because of the area dissipation. Another important set of values is the C-matrix, shown in Equation 4.17. From the C-matrix we can see that the first, third and the fifth coefficients are in the order of femtosiemens. The sixth element of the C-matrix is in the order of millisiemens. The only coefficients that are not negligible are the second and the fourth elements.

$$L = 1.0e - 9 \begin{bmatrix} 0.4 & 1.44 & 3.37 \end{bmatrix} \quad (4.14)$$

$$C = 1.0e - 12 \begin{bmatrix} 2.49 & 0.382 & 0.114 \end{bmatrix} \quad (4.15)$$

$$R = \begin{bmatrix} 218 \end{bmatrix} \quad (4.16)$$

$$C_{mtx} = \begin{bmatrix} 1.12e - 15 & -1 & -1.5e - 15 & 0.218 & 3.82e - 16 & 9.12e - 4 \end{bmatrix} \quad (4.17)$$

4.3 Conclusion

In Section 4.1 different filter topologies are presented and studied. First the well known Gm-C topology is presented. Then high pass and low pass LC topologies are studied. The author proposes to implement the read out factors using the passive part and identical Gm blocks. This topology is shown in Figure 4.3. After this, new topologies, low pass and high pass Gyrator-C, are introduced. From all the abovementioned topologies the low pass LC topology is selected to implement the UWB pulse generator. In Section 4.2 the order of the transfer function is selected. Then the transfer function is translated into inductors, capacitors, resistor and C-matrix values.

Chapter 5

Circuit Design

In Chapter 2 the pulse shape was designed. In Chapter 3 the generation principle was chosen. In Chapter 4 component values for low pass based LC pulse generator were calculated. In Chapter 5 the low pass LC filter based UWB pulse generator is implemented and tested by means of circuit simulations. The low pass LC filter based pulse generator is divided into a Dirac pulse generator, LC filter and states readout circuit (C-matrix), as seen in Figure 5.1.

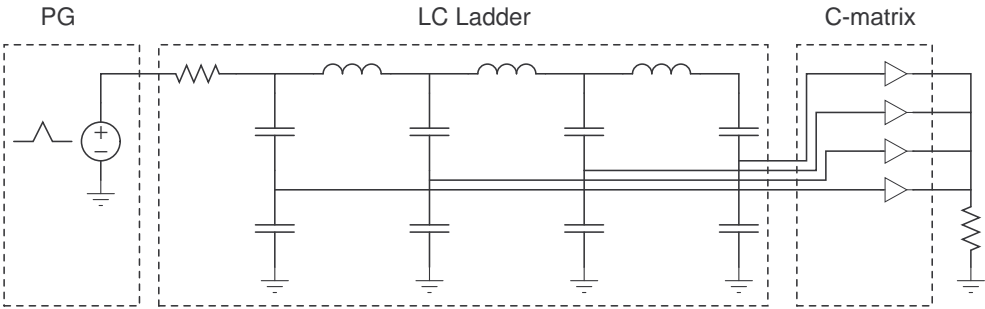


Figure 5.1: UWB pulse generator.

5.1 Dirac Pulse Generator

The dirac pulse generator is implemented using binary circuitry. The clock signal passes through a cascade inverters causing a delay. Then the delayed and non-delayed signals are combined using a NOR circuit. The output of the NOR component is inverted using an inverter which is also used as the interface between the Dirac pulse generator and LC ladder. This inverter is also used to control the peak to peak amplitude of the pulse, in order to fit to the magnitude of the FCC mask. In Figure 5.2 the dirac pulse generator is depicted. Its output voltage is depicted in Figure 5.3.

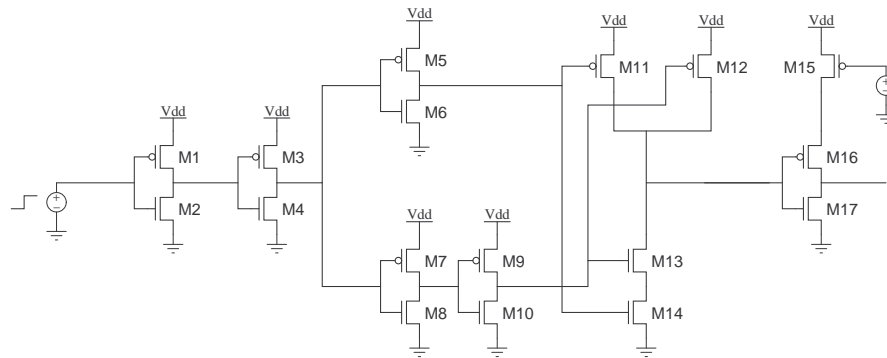


Figure 5.2: Dirac pulse generator.

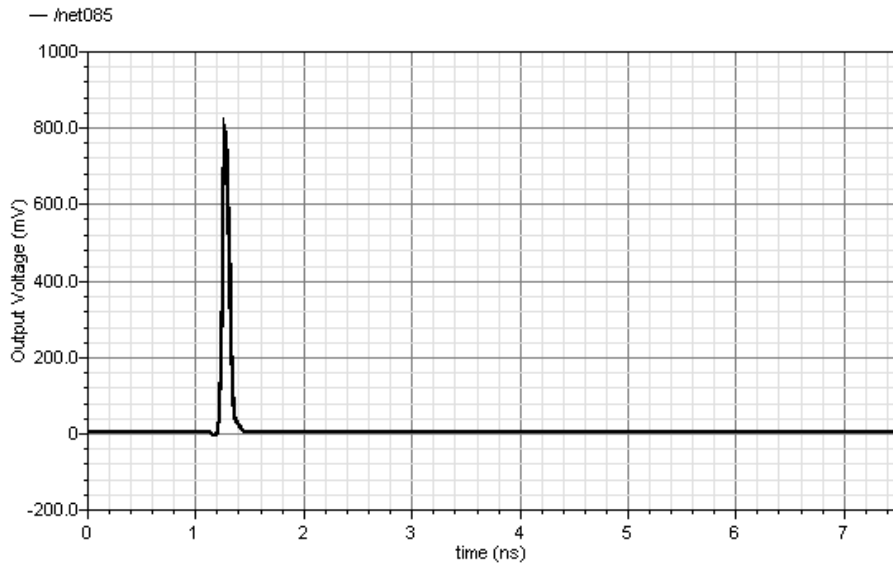


Figure 5.3: Dirac pulse generator's output.

5.2 LC Ladder

The LC ladder is already designed in Chapter 4 and is depicted in Figure 5.4. The L, C and R values are shown below in Equation 5.1, 5.2, 5.3 and 5.4. By replacing the ideal by realistic components, from IBM 0.13 μm technology, the transfer function and so the AC response will be affected. This can result in a pulse generator which is non-compliant with the UWB FCC mask. The realistic inductors and the capacitors are specified in Tables 5.1, 5.2. In Figure 5.5 the AC response of a realistic LC ladder is depicted. From this figure, we can see that the LC ladder is compliant with the FCC mask. Process variation and mismatch is simulated and the result is acceptable as shown in Figure 5.6. The coupling between the inductors can be resolved by the method introduced by [26].

$$L = 1.0e - 9 \begin{bmatrix} 0.4 & 1.44 & 3.37 \end{bmatrix} \quad (5.1)$$

$$C = 1.0e - 12 \begin{bmatrix} 2.49 & 0.382 & 0.114 \end{bmatrix} \quad (5.2)$$

$$R = \begin{bmatrix} 218 \end{bmatrix} \quad (5.3)$$

$$C_{mtrx} = \begin{bmatrix} 1.12e - 15 & -1 & -1.5e - 15 & 0.218 & 3.82e - 16 & 9.12e - 04 \end{bmatrix} \quad (5.4)$$

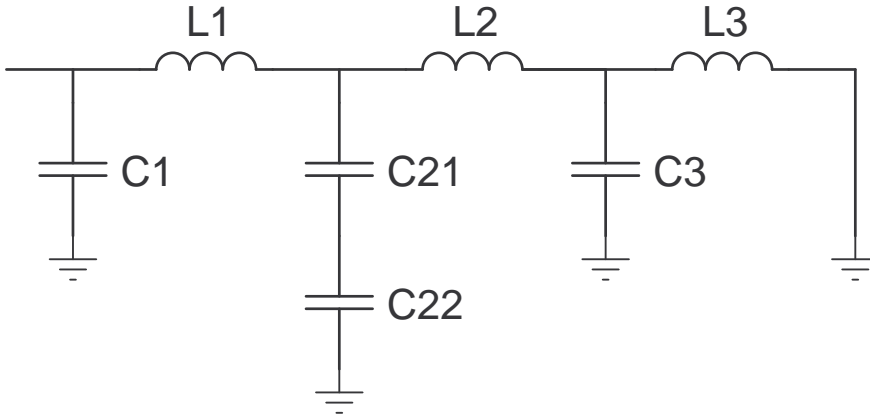


Figure 5.4: LC ladder

Table 5.1: Capacitors specifications

	C1	C21	C22	C3
Cell Name	mimcap	mimcap	mimcap	dualmimcap
Capacitance	114.07f F	488.9f F	1.75p F	2.49p F
Length	8.5u M	8.5u M	8.5u M	8.5u M
Width	6.28u M	27.41u M	98.71u M	39.09u M
Multiplicity	1	1	1	1

Table 5.2: Inductors specifications

	L1	L2	L3
Cell Name	ind	ind	ind
Outer Dimension	190u M	140u M	100u M
Metal Width	5u M	5u M	6u M
n turns	4	3	1.75
Underpass Width	15.0u M	15.0u M	15.0u M
space	5u M	5u M	5u M
Inductance	3.374n H	1.431n H	404p H

5.3 State Readout Circuit

The state readout circuit values were calculated previously and were presented in the previous chapter. See Equation 4.17. The C-matrix values are repeated below in Equation 5.5. From these values we can conclude that only the second state and the fourth state are giving relevant contributions. The other values are negligible. This allows us to connect the LC ladder directly to the next stage. This stage can be a power amplifier or an UWB antenna. In case of an antenna, bondpad and bondwire effect have to be taken into account.

$$C_{mtrx} = \begin{bmatrix} 1.12e - 15 & -1 & -1.5e - 15 & 0.218 & 3.82e - 16 & 9.12e - 04 \end{bmatrix} \quad (5.5)$$

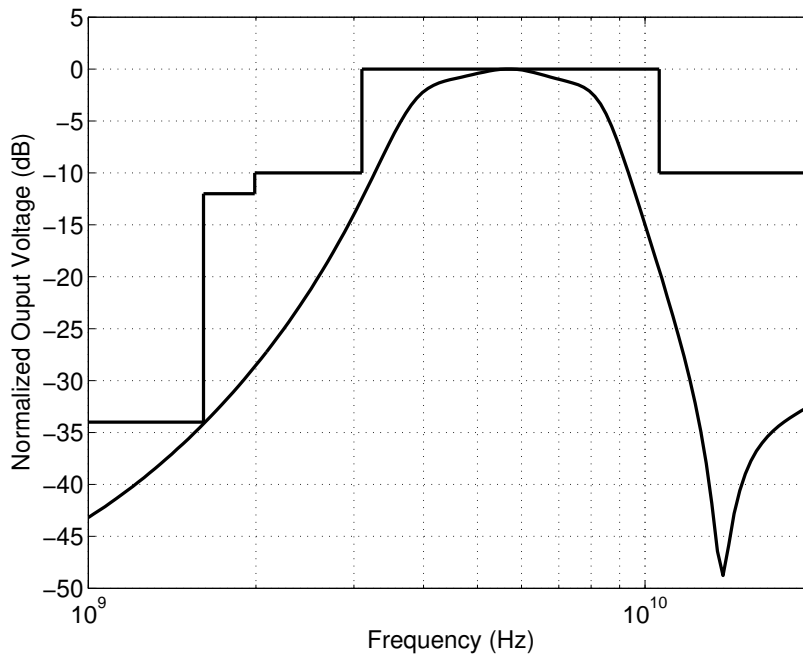


Figure 5.5: AC response of the UWB pulse generator

5.4 Simulation Results

In this section the results of the total circuit, consisting of the dirac pulse generator and the LC ladder, are presented. First, in Figure 5.7, the total circuit is shown. As mentioned above, there are two possible next stages. The next stage is either a power amplifier or an antenna. The loading conditions differ in both cases. Therefore this

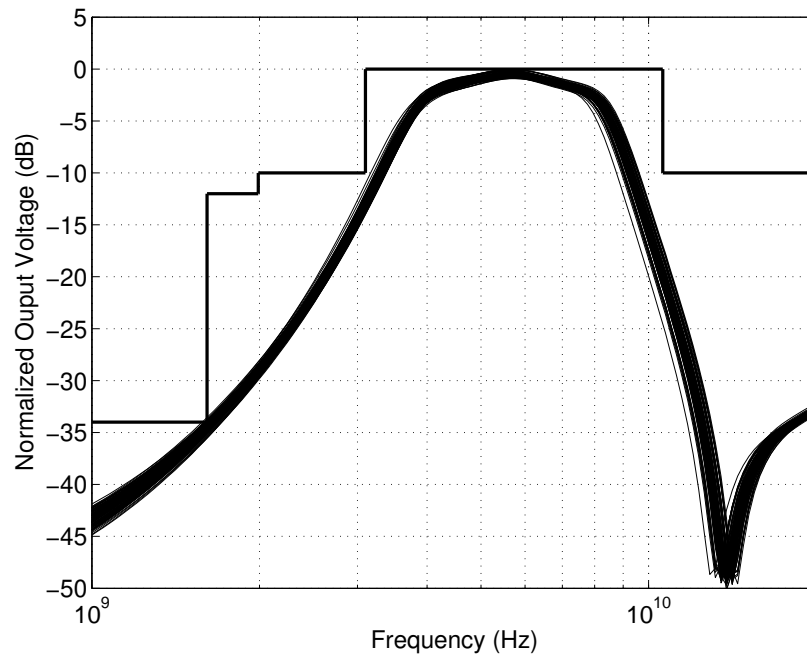


Figure 5.6: Monte Carlo analysis of AC response of the UWB pulse generator

section is divided into two subsection based on the loading conditions.

5.4.1 Simulation results in case of a power amplifier as the next stage

The UWB pulse generated is shown in Figure 5.11. It can be seen that the amplitude is 336.8mV and the duration of the pulse is approximately 2 ns. To check the effect of mismatch and process variations a Monte Carlo simulation is used. The result is shown in Figure 5.13. From this figure we can conclude that the effect of mismatch and process variation on the UWB pulse is acceptable.

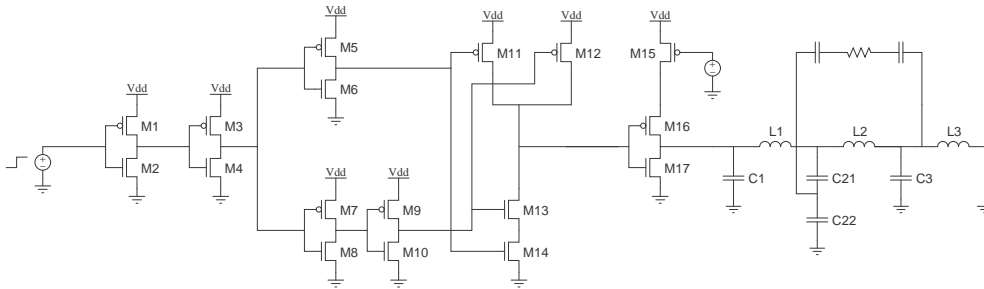


Figure 5.7: Circuit implementation of the UWB pulse generator

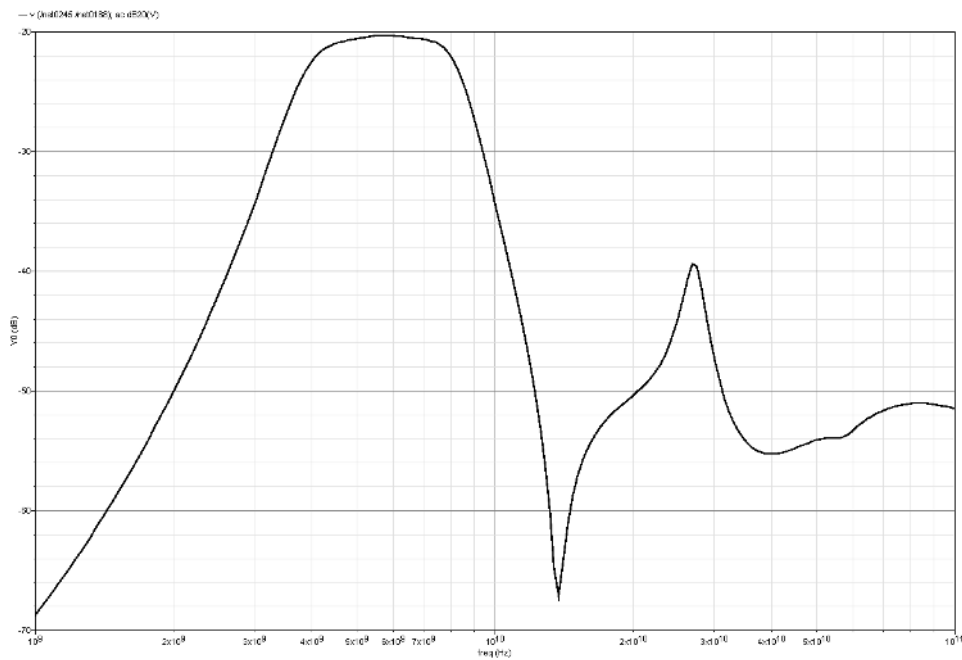


Figure 5.8: AC response of the UWB pulse generator

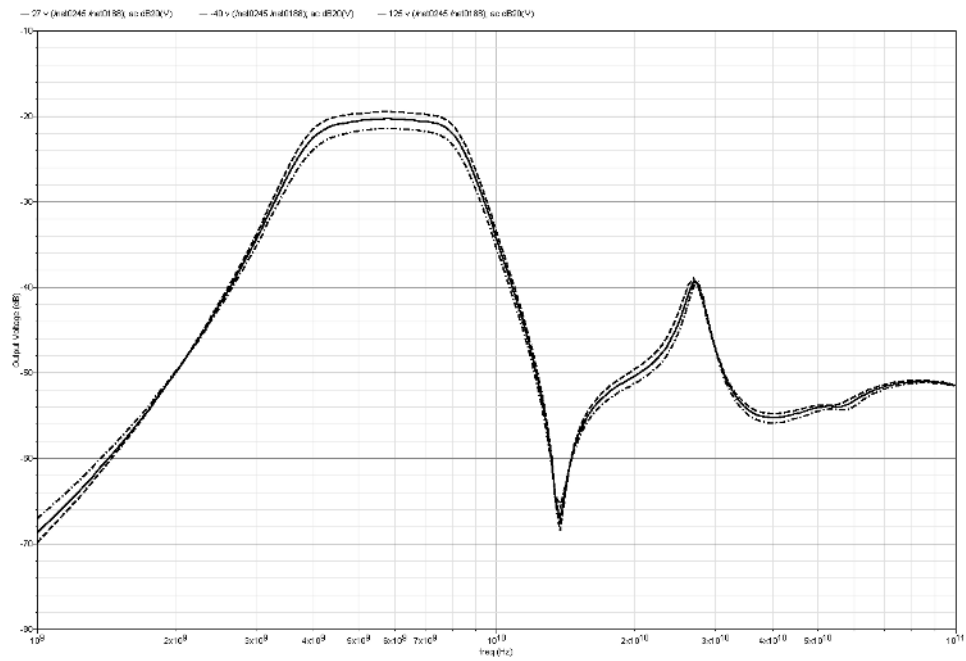


Figure 5.9: AC response of the UWB pulse generator over military temperature range of operation

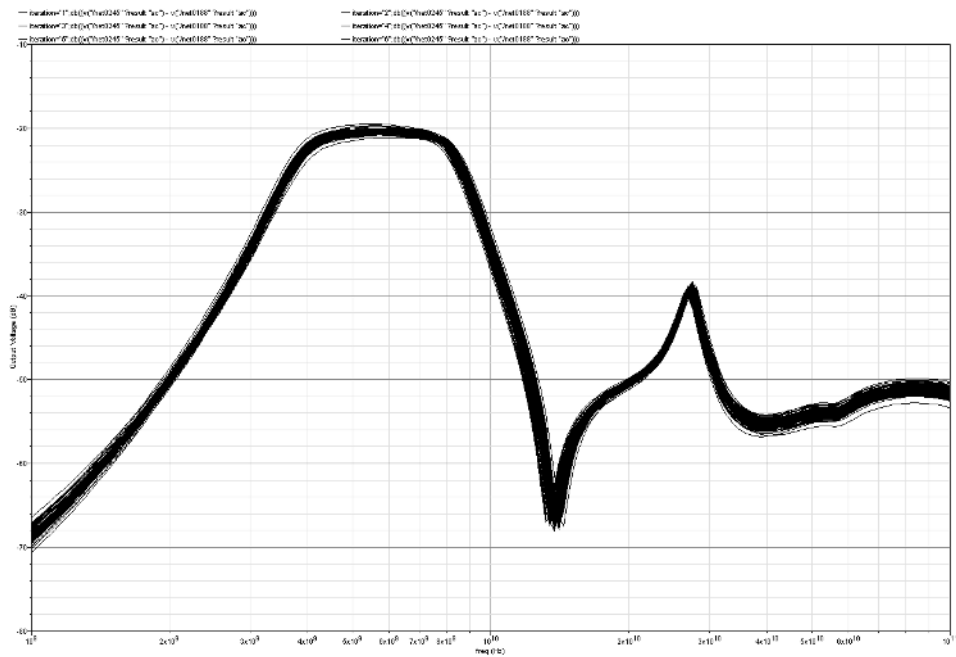


Figure 5.10: The effect of mismatch and process variation on the AC response of the UWB generator

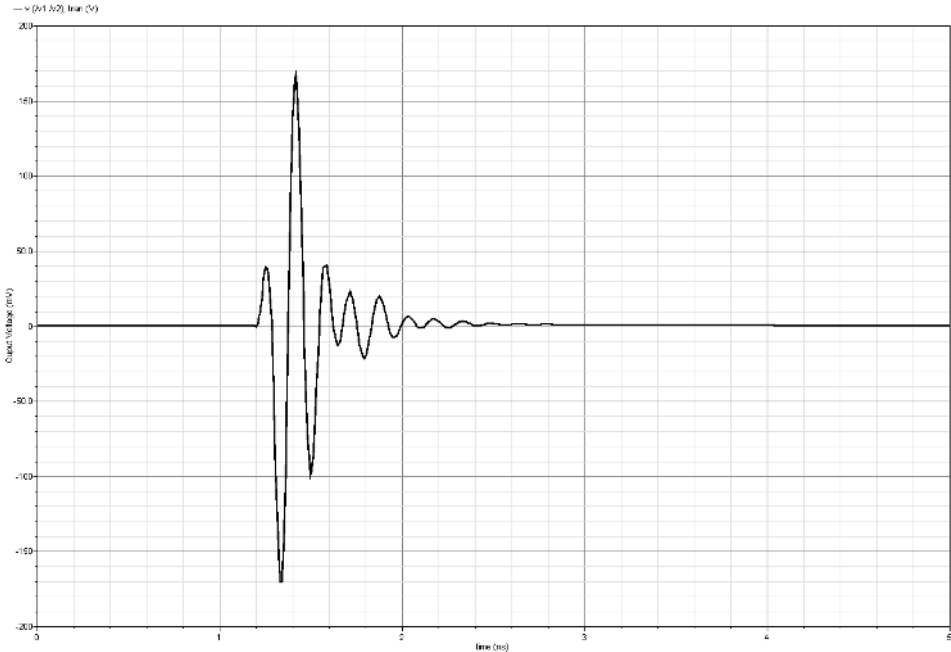


Figure 5.11: UWB pulse generated by transient simulation

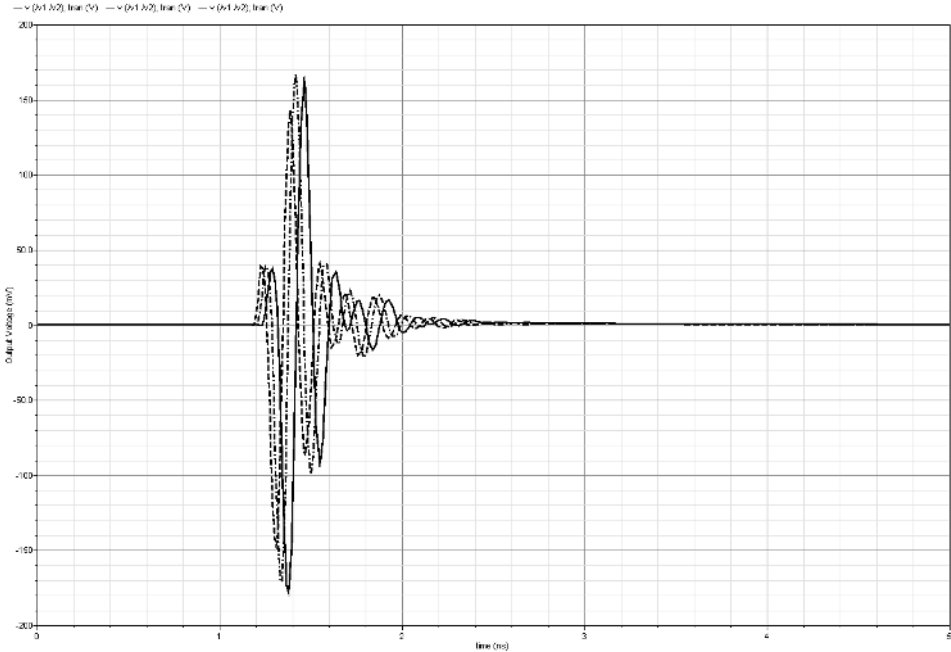


Figure 5.12: UWB pulse over military temprature range of operation

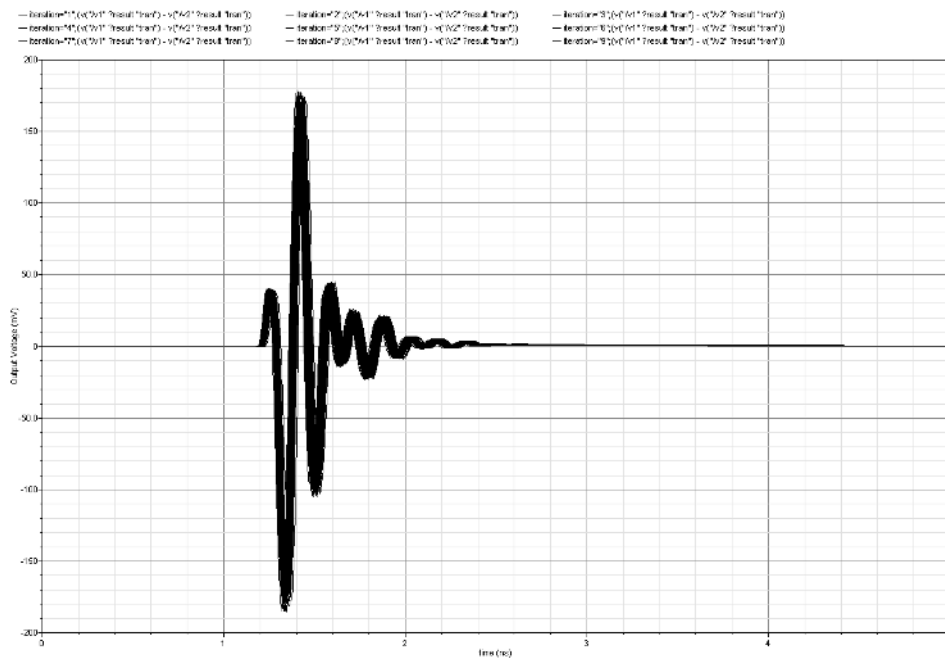


Figure 5.13: The effect of mismatch and process variation on the UWB pulse

To ensure pulse generator's compliance with the UWB FCC mask, a pulse amplitude control is added. The control works by limiting the energy provided by dirac pulse generator to the LC ladder. This is done by varying the V_{dd} of the last inverter. The effect of amplitude control on the UWB pulse is shown in Figure 5.14.

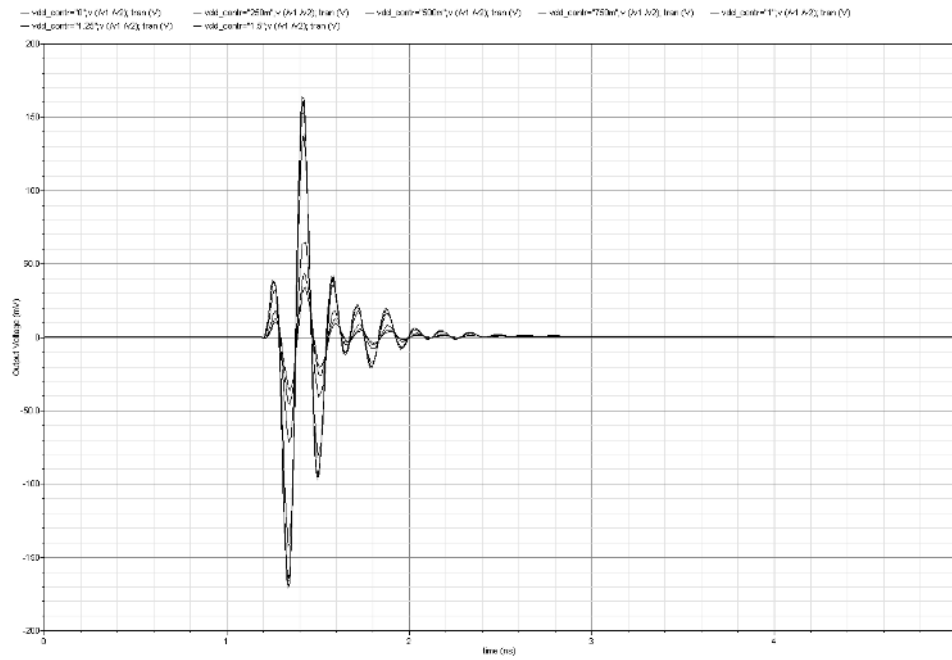


Figure 5.14: UWB pulse amplitude control

5.4.2 Simulation results in case of an antenna as the next stage

In case that the output of the pulse generator is delivered to the antenna directly, the bond pass and the bond wires effect have to be taken into account. The same tests as in the previous subsection are used here. The results are presented in Figures 5.15, 5.16, 5.17, 5.18, 5.19, 5.20 and 5.21.

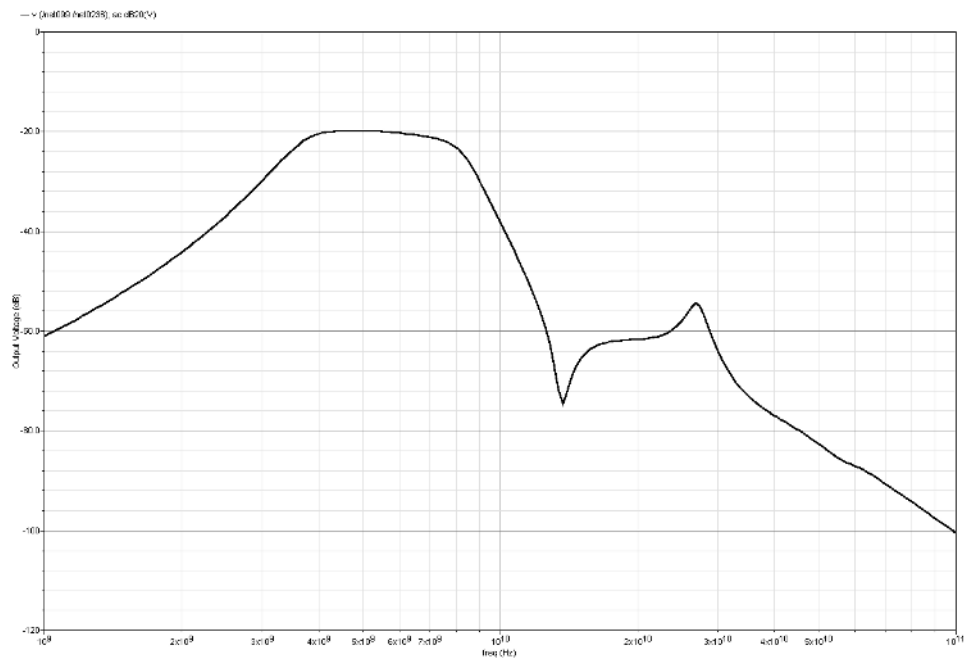


Figure 5.15: AC response of the UWB pulse generator

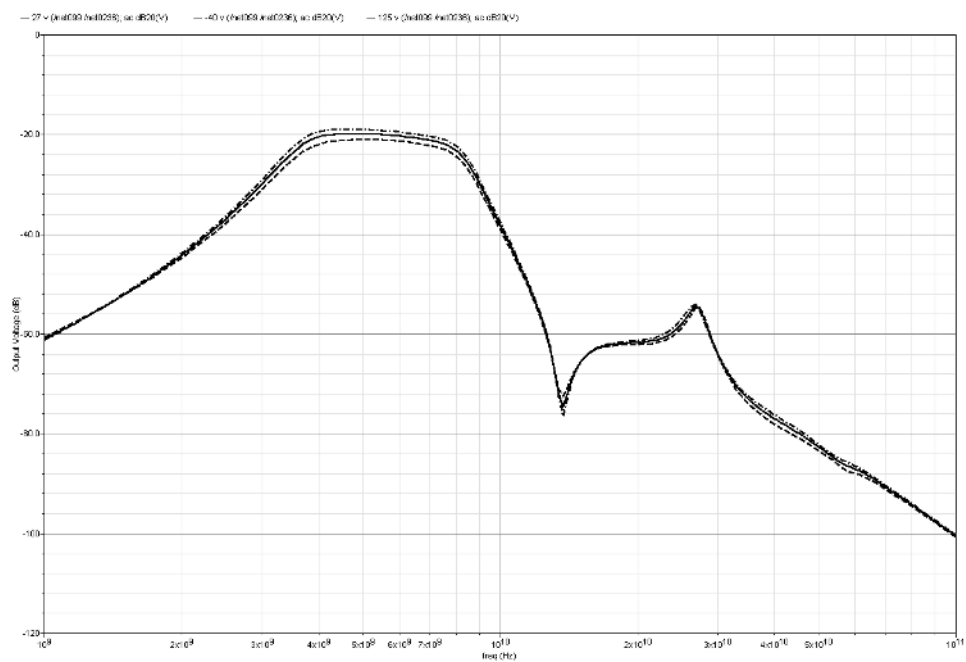


Figure 5.16: AC response of the UWB pulse generator over military temperature range of operation

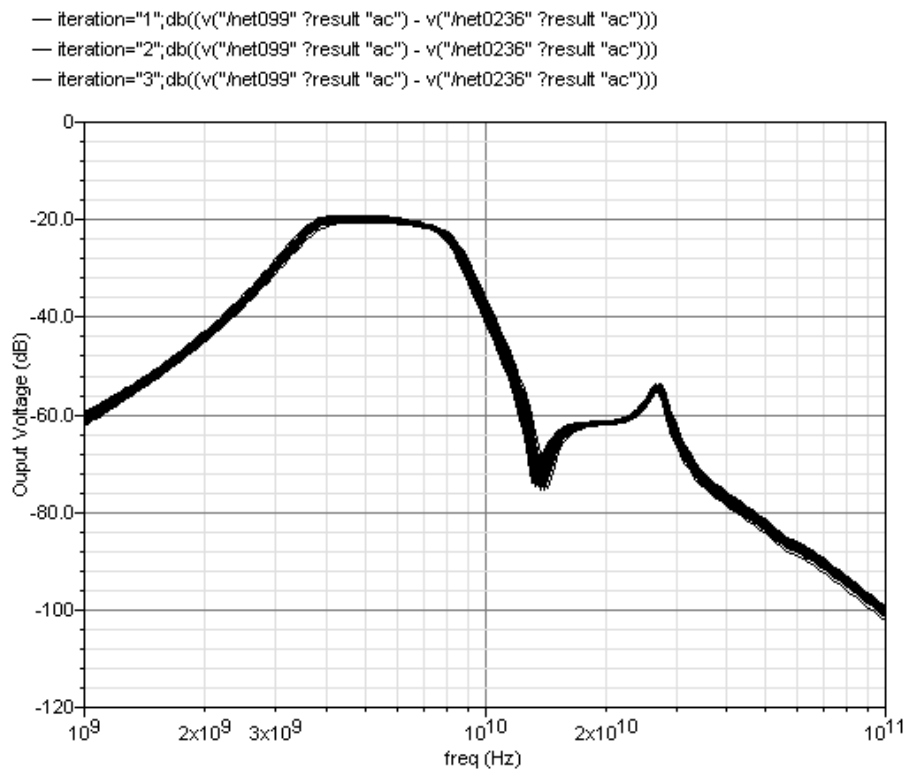


Figure 5.17: The effect of mismatch and process variation on the AC response of the UWB generator

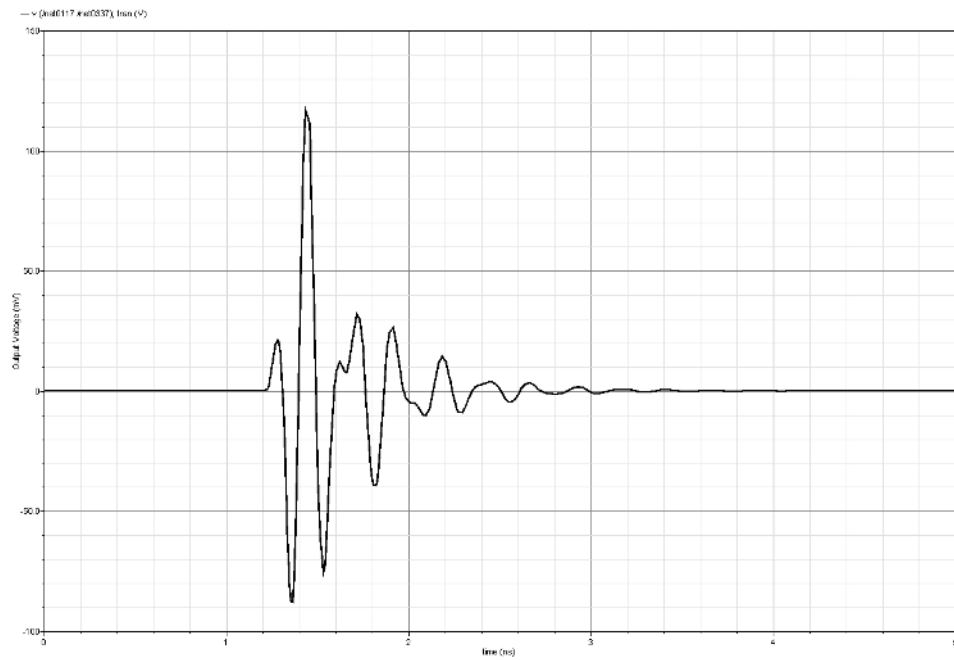


Figure 5.18: UWB pulse generated by transient simulation

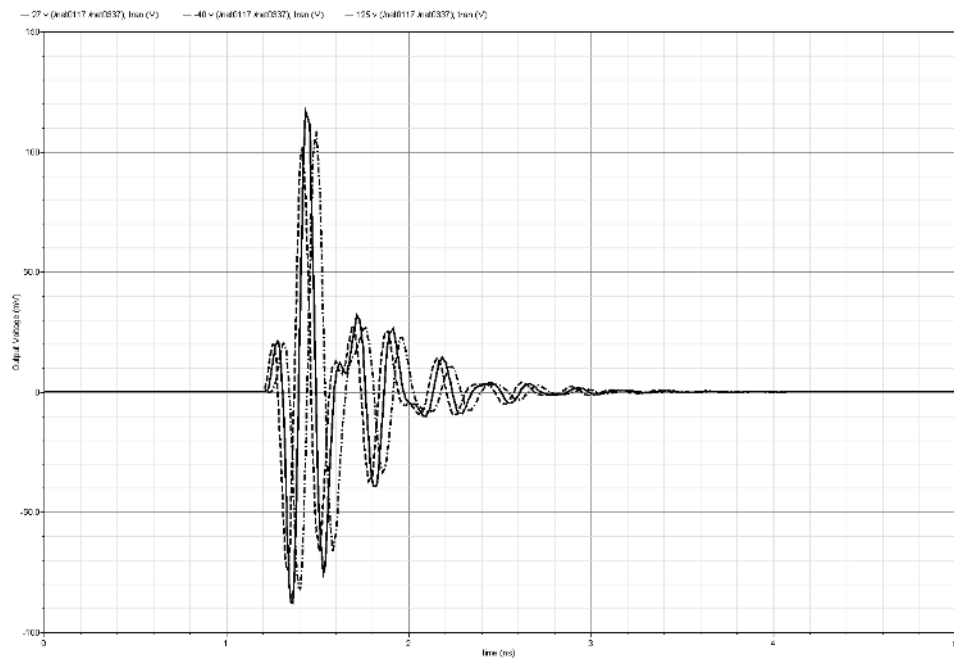


Figure 5.19: UWB pulse over military temperature range of operation

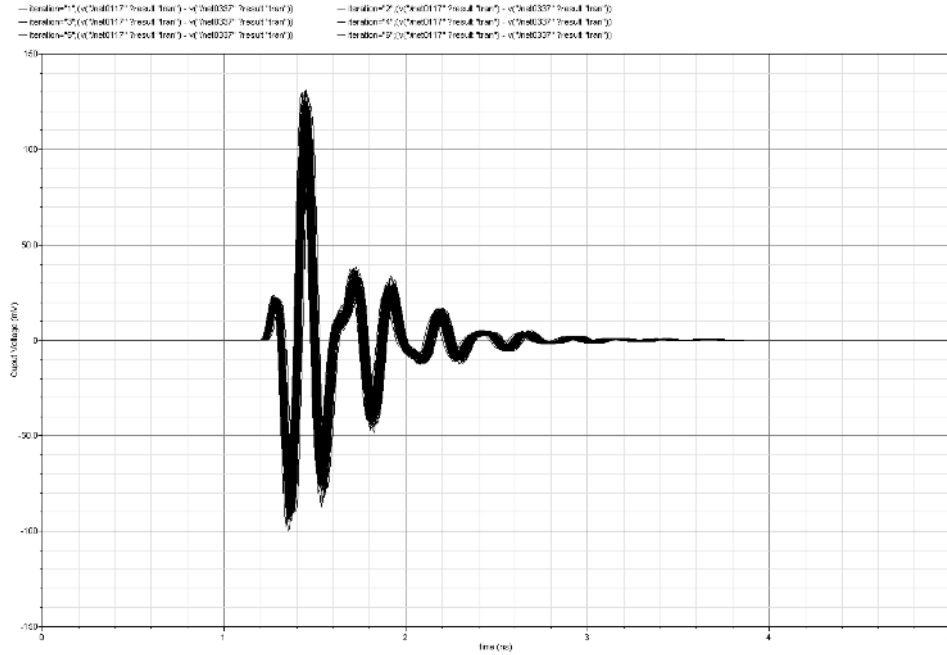


Figure 5.20: The effect of mismatch and process variation on the UWB pulse

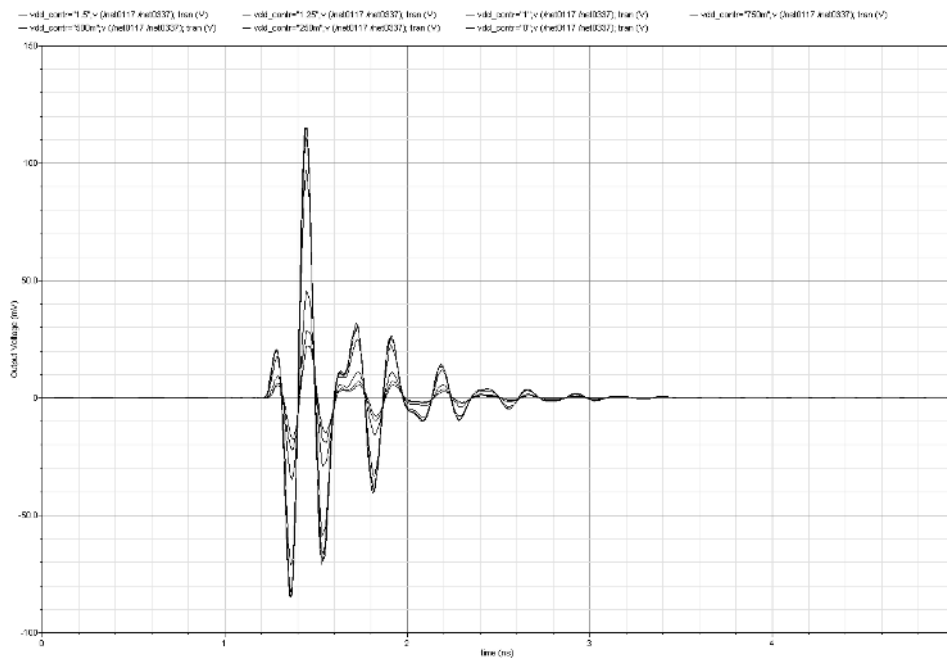


Figure 5.21: UWB pulse amplitude control

5.5 Conclusion

In this chapter the circuit of the low pass LC ladder UWB pulse generator is designed. The pulse generator is divided into a Dirac pulse generator, an LC ladder and a states readout circuit. Dirac pulse generator delays a clock signal with two different delays. The delay elements are realized using inverters. Then the two signals are combined to form a Dirac pulse. The LC ladder is implemented using realistic components from IBM 0.13 μm technology. No state readout circuit is needed, since only two of the six states are non-negligible. Using circuit simulations the effect of using realistic components, temperature variations, mismatch, process variations and amplitude control on transient and AC response of the UWB pulse generator is studied. In Table 5.3 the performances and operating conditions of the circuit is summarized.

Table 5.3: Performance summary

Current consumption per pulse	13mA per pulse
Power consumption per pulse	19.5mW per pulse
Rest current consumption	6mA
Peak to peak amplitude	350mV
Supply voltage	1.5V
Technology	IBM 0.13 μm
Type of input signal	Step
Temperature range	Military temperature range (-40 °C to 125 °C)

Chapter 6

LC Filter States Readout

The LC filter has an important advantage over a Gm-c filter. This is, the state forming is done passively contrary to the Gm-c topology, which makes it a better choice in low power applications. Unfortunately, the area consumption of LC filter is a problem in applications with limited chip area. The states in an LC topology are the voltages over the capacitances and the currents through the inductors. The readout of the voltages is trivial. Reading out the currents through the inductors is more complicated. The problem is formulated as follows: finding a way to read out the current states without affecting the filter. The existing solutions are presented and a novel solution is proposed.

6.1 Previous Solutions

The problem is solved by the authors of [3] using a transformer. This transformer generates a copy of the current at its output. This solution has the disadvantage of using many inductors, which is not area efficient. Another disadvantage is that the impedance seen at the output of the transformer will be translated to the input, causing an impedance in series with the inductors. This causes modification of the transfer function and so the quality of the filter. This solution is depicted in Figure 6.1.

In [4], the author proposes using a dual ladder filter in order to minimize the interference mentioned before and in order not to use a transformer. See Figure 6.2.

There exists another solution which utilizes a sense resistor for converting the current to a voltage. The voltage is then sensed and combined to other states. This topology is shown in Figure 6.3. The problem is that the resistor modifies the filter's

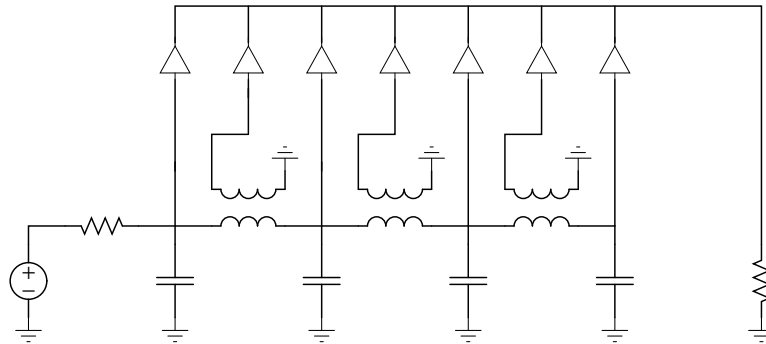


Figure 6.1: Transformer-C filter [3]

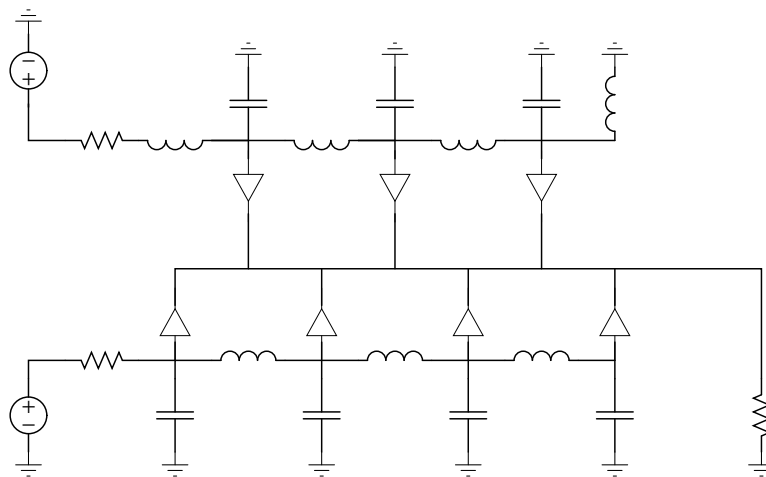


Figure 6.2: Dual ladder filter [4]

transfer function and adds thermal noise.

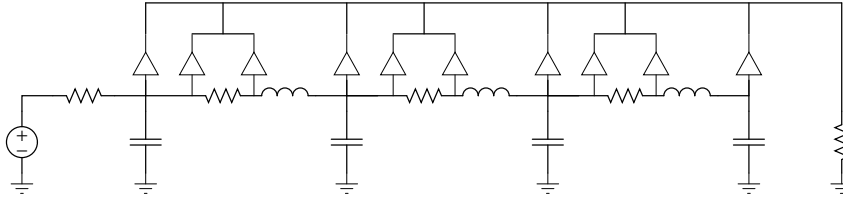


Figure 6.3: Sensing the current using a resistor

6.2 Novel Solution

The solution proposed here utilizes the duality between the inductor and the capacitance. By converting the voltages at both sides of the inductor to currents, subtracting them and integrating the difference, the current in the inductor is translated to a voltage over a capacitor. These steps are shown in Figures 6.4 and 6.5, and in Equations 6.1, 6.2 and 6.4. This solution does not need extra inductors or transformers and does not affect the transfer function of the total filter. This makes this solution preferable to the previous ones. The new topology is depicted in Figure 6.6.

$$I_L = \frac{V_1 - V_2}{Z_L} = \frac{V_1 - V_2}{sL} \quad (6.1)$$

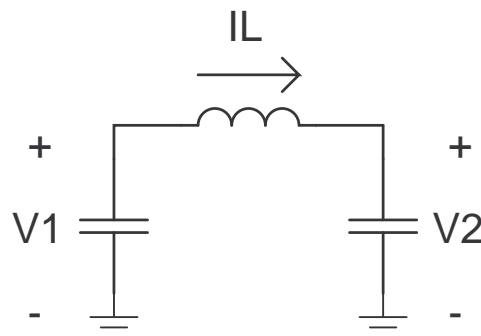


Figure 6.4: The current through an inductor

$$V_C = Z_C(I_1 + I_2) = \frac{I_1 + I_2}{sC} = \frac{g_m V_1 - g_m V_2}{sC} = \frac{g_m}{sC}(V_1 - V_2) \quad (6.2)$$

$$g_m = 1 \quad (6.3)$$

$$V_C = \frac{V_1 - V_2}{sC} \quad (6.4)$$

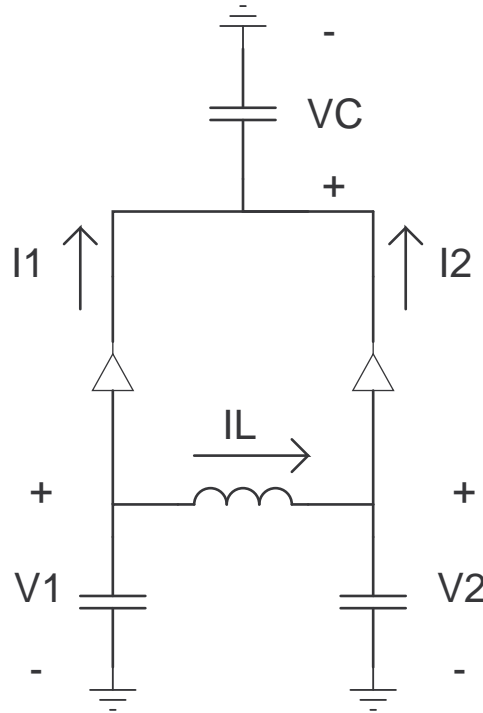


Figure 6.5: A structure to read out the current in an inductor

6.3 Band Rejection Filter Design

In this section a band rejection filter for UWB applications is designed using the new topology discussed in the chapter. The filter aims to reject the Wireless Local Area Network (WLAN) frequency of 5.5 GHz.

6.3.1 Matlab Design

Using the “`ellip`” function in Matlab, a 4th order filter is designed. The magnitude bode diagram of the filter is shown in Figure 6.7. In Equations 6.5, 6.6, 6.7 and 6.8 the state space description of the filter is seen. As seen before this state space has to be translated to orthonormal form. The orthonormal state space is shown in Equations

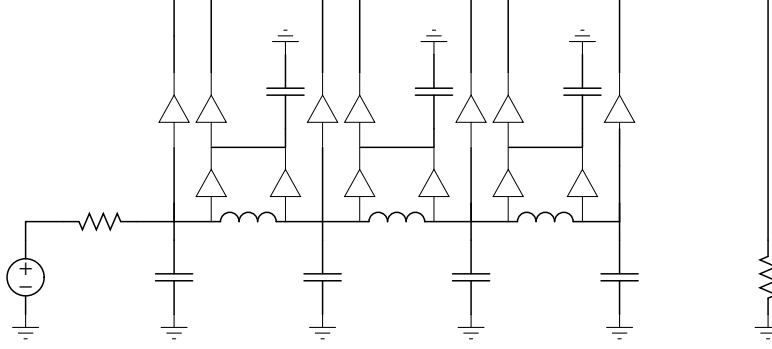


Figure 6.6: A filter utilizing the structure to sense the current in an inductor

6.9, 6.10, 6.11 and 6.12. This state space has some disadvantages. First there are 3 non-neglectable values in the C matrix. Another disadvantage is the D matrix. In total there are 4 outputs, thus 4 readout stages are needed to realize this filter. By examining the individual states, in Figure 6.8, an interesting state is noticed. The 4th state forms a possible alternative for the total filter. The 4th state is depicted together with the total filter in the bode diagram in Figure 6.9. The AC response of the state is not flat outside the rejected region, but the deviation in the frequencies of interest is small. From this, we can conclude that the 4th state has an acceptable frequency response.

$$A = \begin{bmatrix} -3.96e + 10 & -3.46e + 21 & -4.69e + 31 & -1.4e + 42 \\ 1 & 0 & 0 & 0 \\ 0 & 1 & 0 & 0 \\ 0 & 0 & 1 & 0 \end{bmatrix} \quad (6.5)$$

$$B = \begin{bmatrix} 1 \\ 0 \\ 0 \\ 0 \end{bmatrix} \quad (6.6)$$

$$C = \begin{bmatrix} -3.8e + 10 & -1.05e + 21 & -4.5e + 31 & -3.65e + 30 \end{bmatrix} \quad (6.7)$$

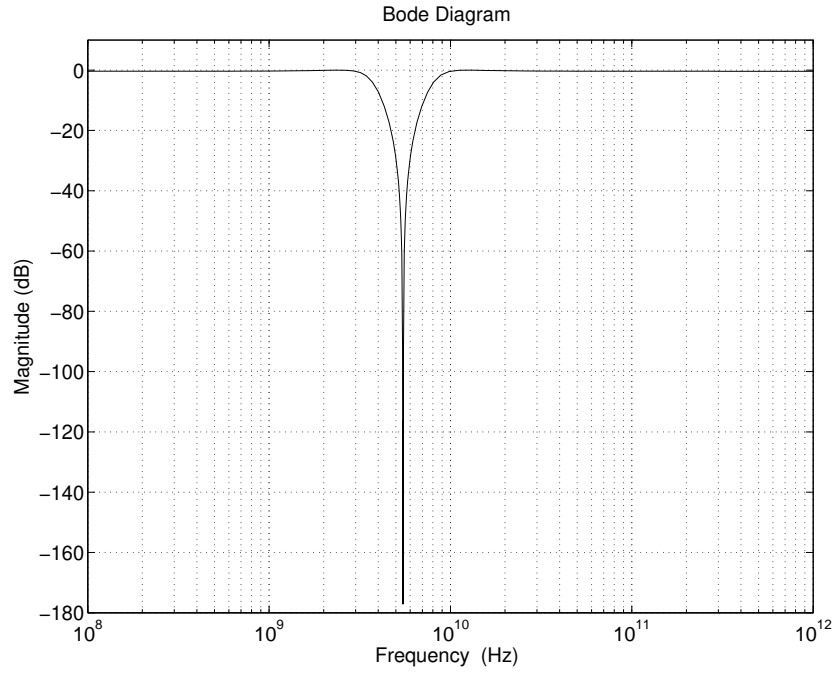


Figure 6.7: Magnitude bode diagram of the ideal band rejection filter design

$$D = \begin{bmatrix} 0.959 \end{bmatrix} \quad (6.8)$$

$$A = \begin{bmatrix} 0 & 2.48e + 10 & 0 & 0 \\ -2.48e + 10 & 0 & 2.38e + 10 & 0 \\ 0 & -2.38e + 10 & 0 & 4.77e + 10 \\ 0 & 0 & -4.77e + 10 & -3.96e + 10 \end{bmatrix} \quad (6.9)$$

$$B = \begin{bmatrix} 0 \\ 0 \\ 0 \\ 1.12e + 05 \end{bmatrix} \quad (6.10)$$

$$C = \begin{bmatrix} 2.04e + 05 & 4.34e - 05 & -1.95e + 05 & -3.38e + 05 \end{bmatrix} \quad (6.11)$$

$$D = \left[0.959 \right] \quad (6.12)$$

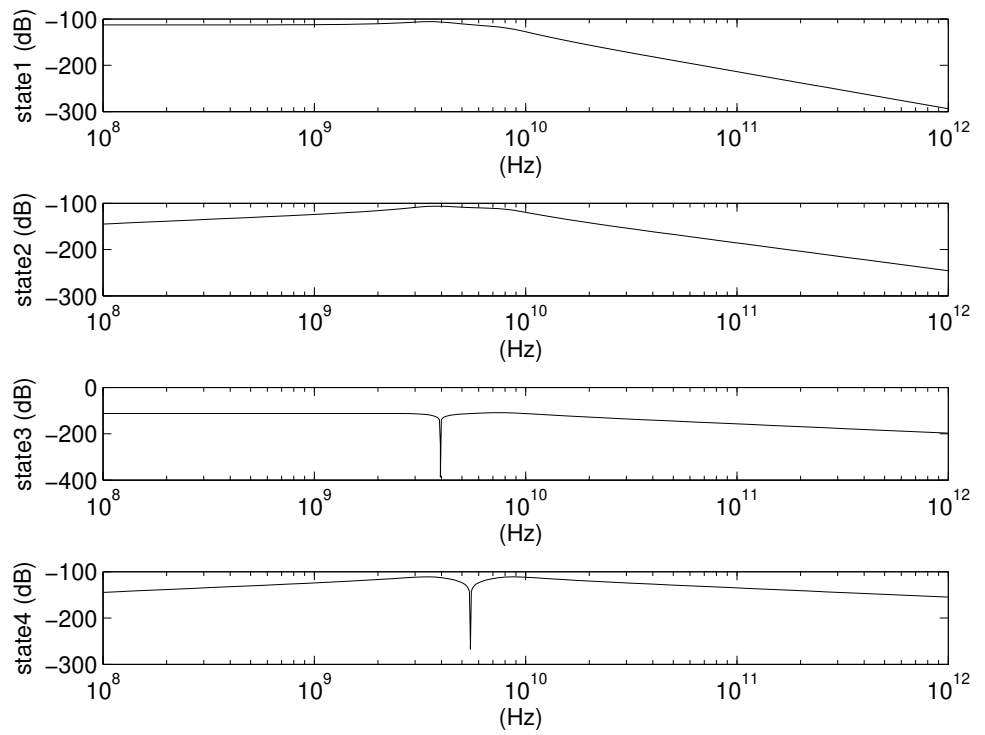


Figure 6.8: Filter's states magnitude bode diagram

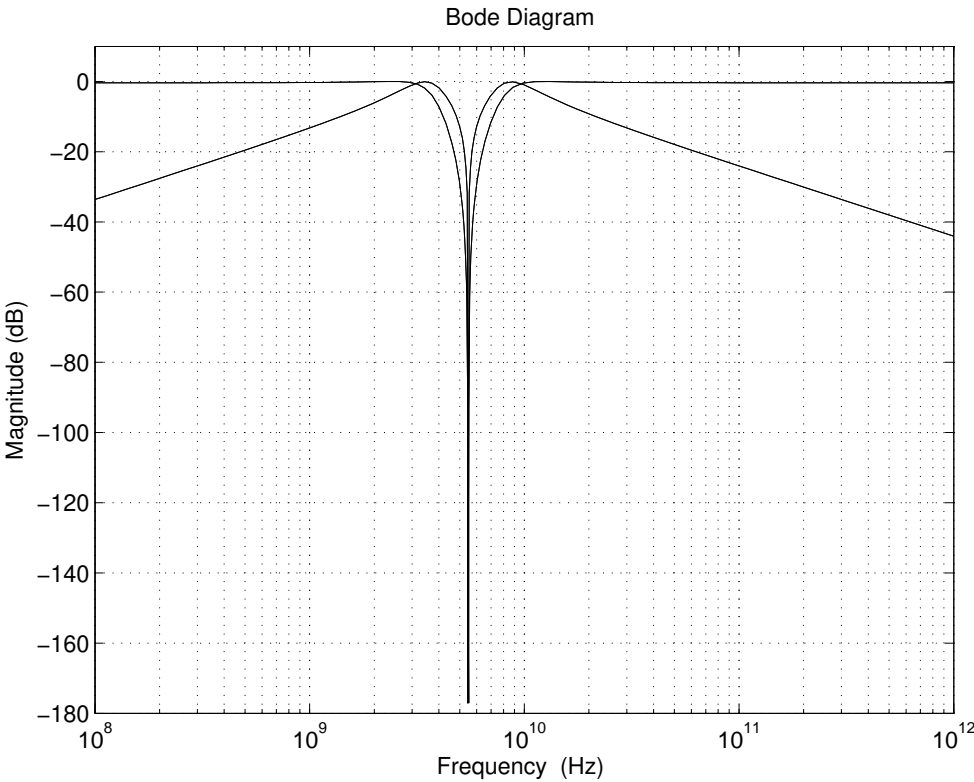


Figure 6.9: AC response of the total filter and the 4th state of the filter

In this section, the 4th state of the filter is chosen as the output of the filter. The 4th state can be implemented as a voltage over a capacitance or as a current through an inductor. This is shown in respectively Figure 6.10 and 6.11. The first possibility is easier but to test the new topology the second possibility is designed in the next section.

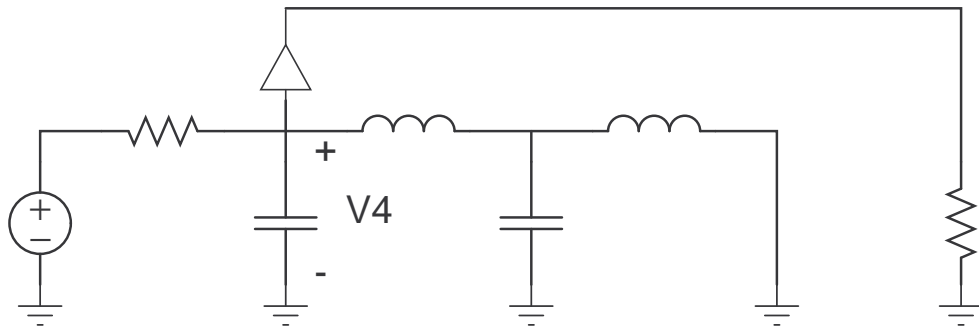


Figure 6.10: The 4th state as a voltage over a capacitor

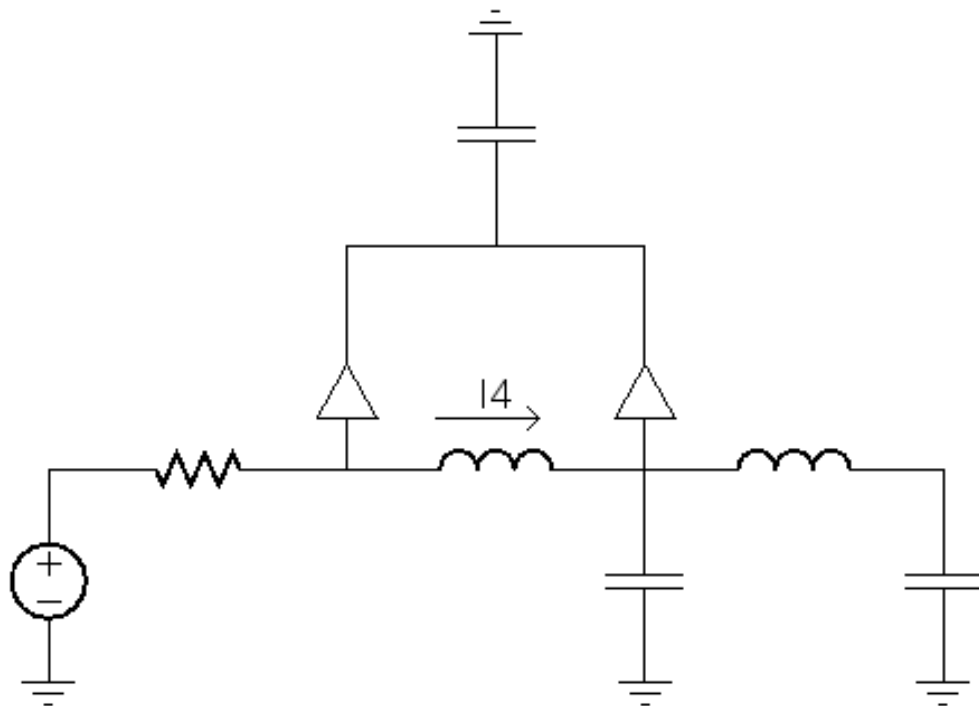


Figure 6.11: The 4th state as a current through the inductor

6.3.2 Circuit Design

In Figure 6.12 the circuit implementing the band rejection filter is shown. The circuit consists of an LC ladder, readout of the voltages on both sides of the inductor and the output is differential over the two integrating capacitors. In Table 6.1 the capacitors specifications are presented. Then in Table 6.2 the inductors specifications are presented.

In Figure 6.13 the AC magnitude response of the filter is depicted. The depth of filter's notch is 17 dB. The other two notches are located outside frequencies of interest for the UWB systems. When tested over the military temperature range (-40 °C, 27 °C and 125 °C) the AC response shape does not change. The notch depth and the position of the low frequency notch is changed, as depicted in Figure 6.14. To test process variation and mismatch Monte Carlo analysis is used. The result is shown in Figure 6.15. The mismatch and process variation affect merely the low frequency notch.

Table 6.1: Capacitors specifications

	C1	C2	C3	C4
Cell Name	dualmimcap	dualmimcap	dualmimcap	dualmimcap
Capacitance	2.17p F	2p F	680.17f F	680.17f F
Length	8.5u M	8.5u M	8.5u M	8.5u M
Width	33.75u M	30.87u M	8.5u M	8.5u M
Multiplicity	1	1	1	1

Table 6.2: Inductors specifications

	L1	L2
Cell Name	ind	ind
Outer Dimension	100u M	100u M
Metal Width	5u M	5u M
n turns	1	3.25
Underpass Width	15.0u M	15.0u M
space	5u M	5u M
Inductance	210p H	818p H

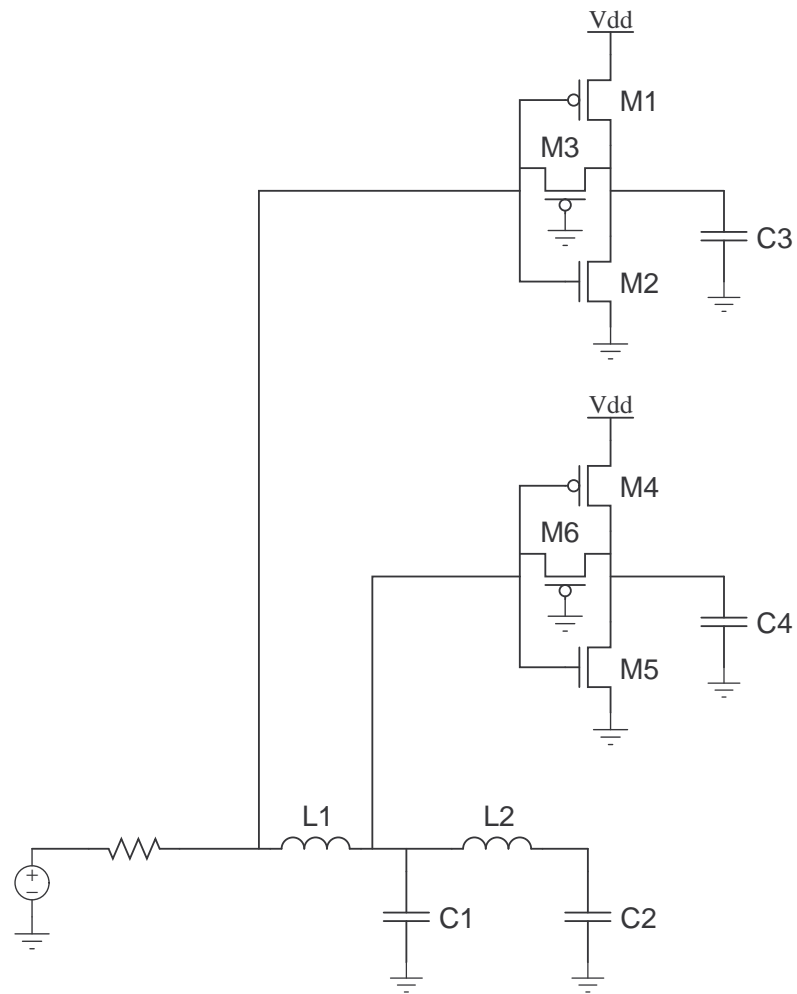


Figure 6.12: Band rejection filter circuit

Table 6.3: Transistors specifications

	M1	M2	M3	M4	M5	M6
Cell Name	pfet	nfet	pfet	pfet	nfet	pfet
Width Single Finger	160n M	160n M	160n M	160n M	160n M	160n M
Width All Fingers	160n M	160n M	160n M	160n M	160n M	160n M
Length	120.0n M	120.0n M	120.0n M	120.0n M	120.0n M	120.0n M
Number of fingers	1	1	1	1	1	1
Multiplicity	1	1	1	1	1	1

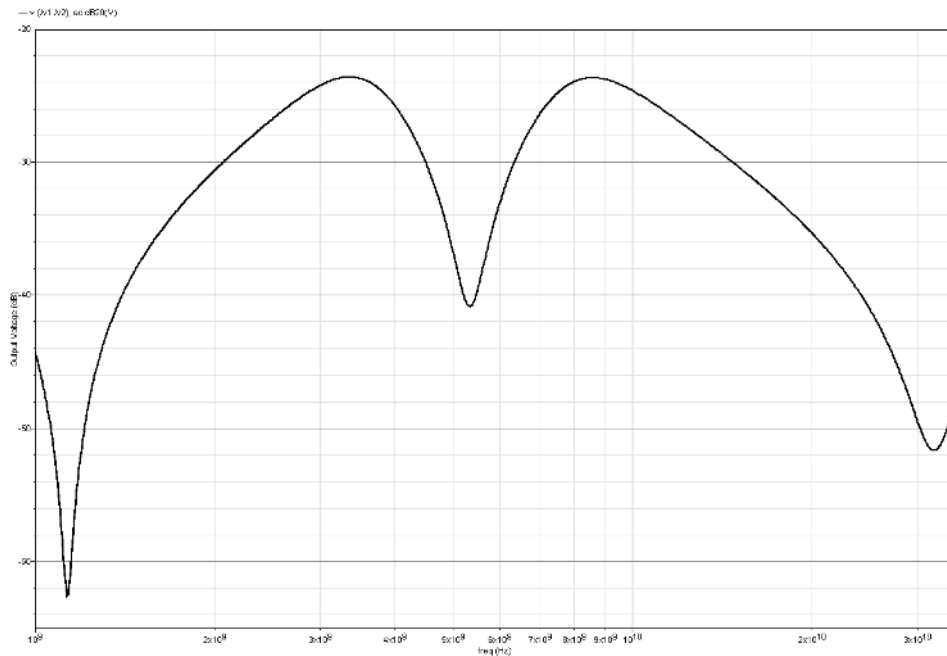


Figure 6.13: AC response of the band rejection filter

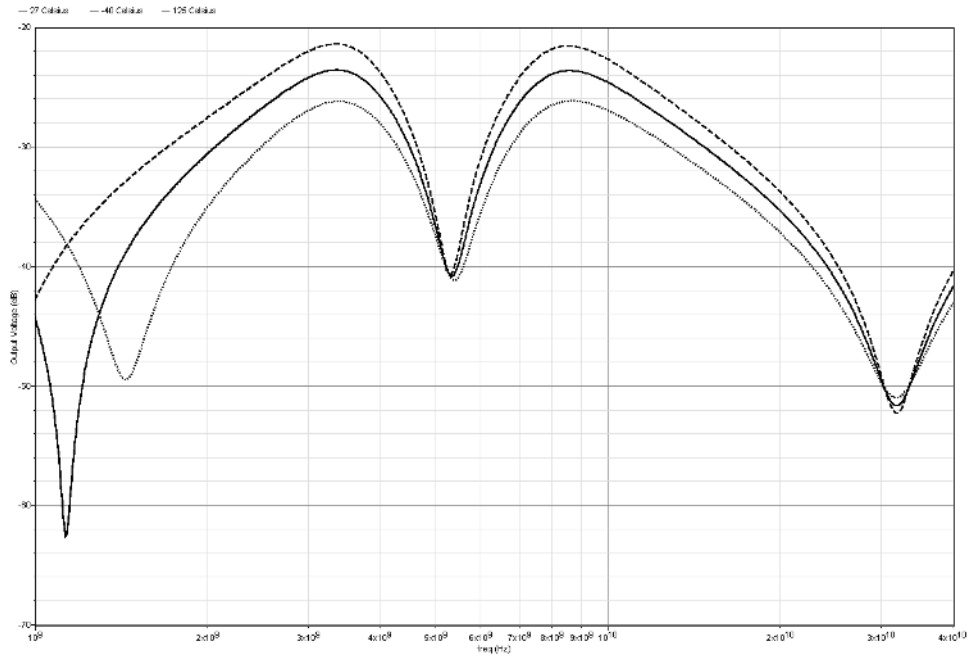


Figure 6.14: AC response over military temperature range of operation.

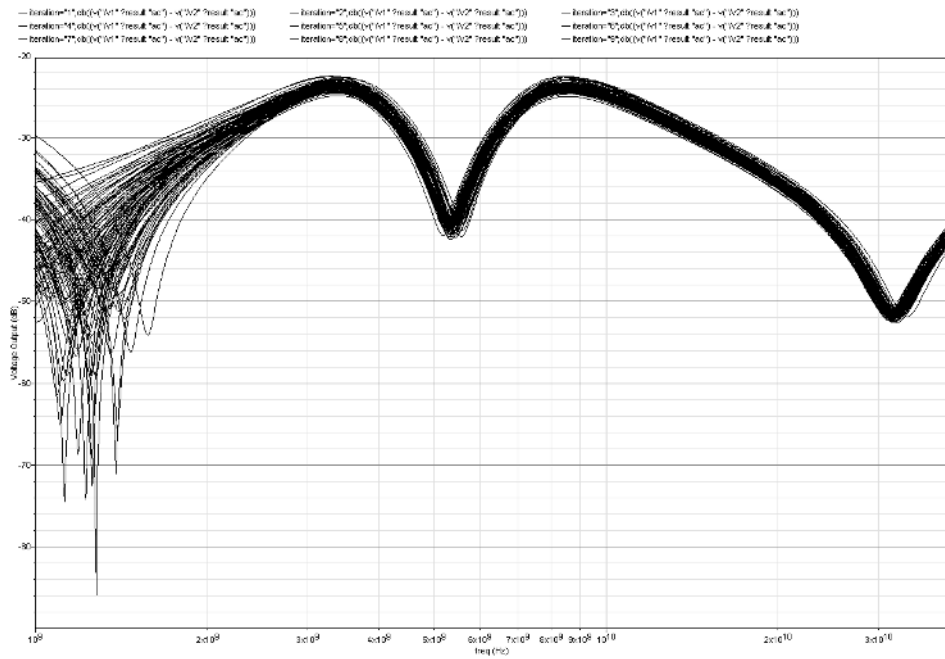


Figure 6.15: The effect of mismatch and process variation on the AC response

The impulse response of the filter is depicted in figure 6.16.

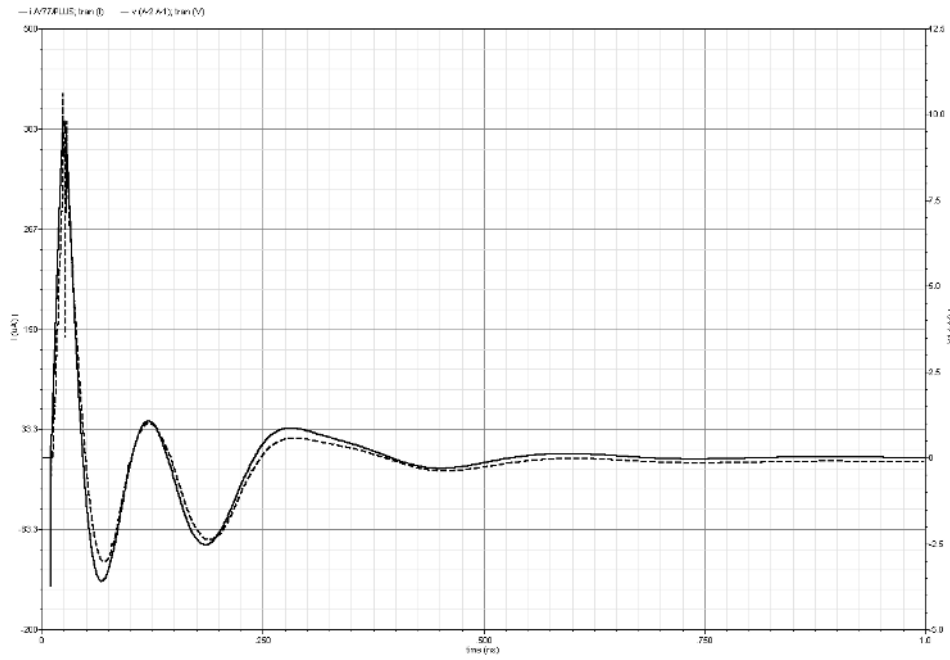


Figure 6.16: Impulse response of the band rejection filter

6.3.3 Conclusion

In this chapter a new filter topology is designed. The new topology enables us to read all the states of the LC filter (the voltages and the currents). A WLAN (5.5 GHz), 4th order, band rejection filter is designed using the new topology in IBM 0.13 μm technology. Then the effect of temperature variations, mismatch and process variations on the filter is studied. Finally the impulse response of the filter using realistic components is compared to the ideal filter. Notch depth of the filter at 27

Table 6.4: Performance summary

Filter Type	Band-reject
Order	4
Bandwidth lower-band	2.5-4 GHz
Bandwidth upper-band	7-12 GHz
Notch depth at 27 °C	17 dB
Notch depth at -40 °C	19 dB
Notch depth at 125 °C	15 dB
Termination input	Single-ended
Termination output	Differential
Supply voltage	1.5V
Technology	IBM 0.13 μm

Chapter 7

Conclusions and Future Work

7.1 Conclusion

In this thesis an LC filter based UWB pulse generator is designed in IBM 0.13 μm technology. First, in Chapter 1, the UWB technology is introduced. The UWB regulations in different regions of the world are presented. Then UWB applications, types and standards are presented. Finally, Impulse Radio UWB is defined and categorized. In Chapter 2 different pulse shapes are compared. Then figures of merits to select pulses are developed. Finally, a pulse shape is selected. Then in Chapter 3 different types UWB pulse generators are compared and filter based pulse generator is selected to be implemented in this thesis. In Chapter 4 different filter topologies are studied. First the well-known Gm-C filter is studied. Then low pass and the high pass LC filter is presented. A novel topology called Gyrator-C filter is introduced. This topology replaces the inductors by active inductors implemented using a gyrator and a capacitor. The above mentioned filters are compared and low pass LC filter is selected to implement UWB pulse generator. To simplify the design of the filter, a new topology derived from the low pass LC filter is introduced. In the new topology the C-matrix is implemented using the passive elements by voltage division. The read-out Gm blocks are made identical. This topology simplifies the design because only one Gm block have to be designed. In the same chapter the order of the filter is selected and the transfer function is translated to L, C, R and C-matrix coefficients. Then in Chapter 5 the circuit is designed. The circuit consists of a Dirac pulse generator and LC ladder. No readout circuit is needed because only two elements of the C-matrix are non-negligible. Dirac pulse generator is designed by delaying the clock signal with different delays then the two delayed signals are combined. The last stage

of the generator controls the peak value of the pulse. LC ladder is implemented using realistic components from IBM 0.13 μm technology. Finally, the effect of temperature variations, process variations and mismatch on the system is evaluated using circuit simulations. Also the amplitude control of the UWB pulse is shown. Finally, in Chapter 6 a problem of the LC filter is presented. The problem is the difficulty of reading out the current states in the inductors. This problem is solved by utilizing the duality between the inductor and the capacitor to convert the current through the inductor to a voltage over a capacitor. Using the new topology a WLAN (5.5 GHz) band-rejection filter is designed and simulated.

7.2 Own Contributions

My own contributions exists from a novel topology filter (Gyrator-C). This filter has less number of active elements comparing to the well-known Gm-C filter and shares the advantage of not using inductors with Gm-C filter. A novel way to read current through inductors in an LC filter is introduced. This technique allows the designer in using all the states of the LC filter to construct the transfer function.

7.3 Future Work

Further study on filter topologies to achieve lower number of active elements and thus lower power consumption. It is also important to study new ways to readout the currents through the inductors to increase the complexity of the implemented filters without increasing the order of the filter. Another issue is the design of low power Gm blocks to decrease the power consumption of the filters.

Appendix A

A discussion on antenna-LNA interface

This chapter is a result of collaboration with Yixiong Hu, M.Sc. student in the class of 2006-2008.

A.1 Introduction to impedance match

Conventional monolithic microwave integrated circuit (MMIC) application requires conjugate impedance matching between components for maximum power transfer from the source to the load. In order to facilitate the independent design of different components, most microwave designs are based on a standard interface impedance of 50Ω . Integrated-circuit implementations have already abandoned this antiquated requirement. For on-chip implementations, the connections between circuit blocks are typically much less than the signal wavelength. Thus transmission line effects can be neglected [27].

Though the output of an LNA is connected to on-chip blocks and thus does not require an impedance match, the LNA 50Ω input impedance match is still required for several reasons. First, it avoids the reflections over the transmission line feeding the LNA causing inter symbol interference (ISI) [28]. Second, it supplies a correct termination for the possible prefilter preceding the amplifier.

While the connection between the receiving antenna and the receiver chip also becomes smaller, the transmission line effects between antenna and LNA can be neglected as well if the connection distance is much less than the signal wavelength. In the AIR-LINK project, the differential antenna is connected directly to the chip with

no filter inserted, which reveals the possibility of tolerance of a mismatch between antenna and LNA input.

Since signal is usually added on the transistor gate as a voltage source to drive the amplifier, LNAs actually sense the signal voltage rather than the power. Thus, it may be interesting to have an open circuit which receives the maximum voltage rather than the maximum input power. LNA gain can be improved if designed with a mismatched input.

Before testing this possibility, power match is discussed. Then an example of mismatched antenna-LNA interface is given. EM Simulation results are shown to indicate that more voltage can be sensed across a transistor capacitor in a mismatched case than a matched case.

A.2 Power match

The conventional explanation on how maximum power transfer can be converted into maximum voltage transfer is given below:

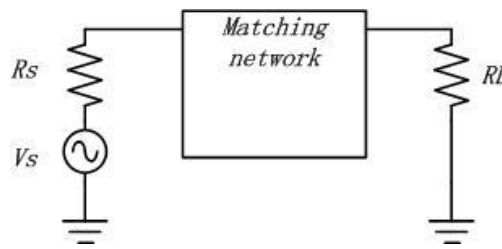


Figure A.1: Matching network for fixed source and load to maximize voltage transfer

The matching network is inserted to achieve an impedance transformation thus the maximum power $P_{max} = V_s^2/4R_s$ is transferred to the load. For a fixed load, the voltage also reaches maximum $V_L = \sqrt{P_{max}R_s}$.

Indeed, for a fixed load, maximum power transfer brings maximum voltage transfer. However, the transistor has a capacitive input, to obtain more voltage on the capacitive load is the goal for maximum gain of a transistor amplifier. If this capacitive load is taken as in parallel with a huge resistive load, a matching network is still possible to be inserted to achieve maximum voltage transfer. However, this parallel resistor in reality is seldom accurate and it takes impractical values of passive component to achieve this power match.

To fulfill the impedance match, usually a resistive part is created intentionally by circuit designers. This type of match is different from the power match concept of the insertion of a passive matching network. It indeed eases the selection of passive components for further impedance matching, for example, a 50Ω resistive termination makes the matching network quite easy just by adding a parallel inductor to tune out the capacitance on one frequency and thus achieves narrowband matching.

Inductively source-degenerated topology also introduces an extra resistive part to achieve input impedance match. However, the following analysis indicates that a higher total transconductance can be obtained if an inductively source-degenerated amplifier has a mismatched input.

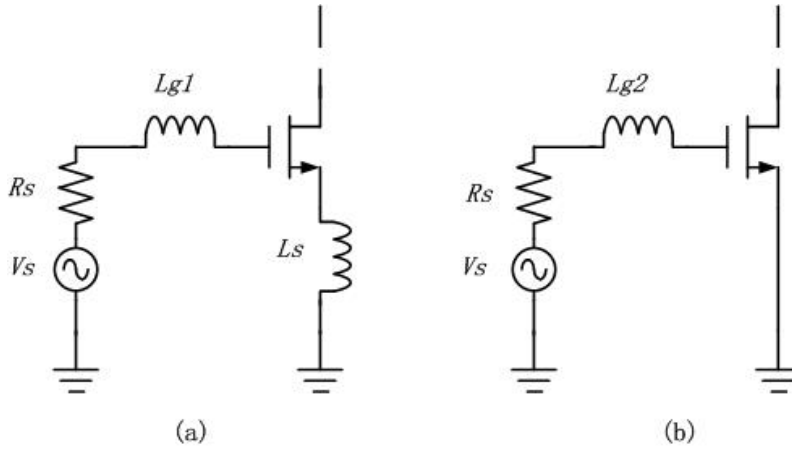


Figure A.2: (a)Inductively-degenerated LNA and (b)resonating common source LNA

Assuming the same C_{gs} and resonant frequency. The total transconductance of (a) and (b) is given as

$$G_{m,a} = \frac{g_m}{2j\omega C_{gs}R_s}$$

$$G_{m,b} = \frac{g_m}{j\omega C_{gs} R_s}$$

respectively.

The total transconductance of the mismatched LNA is twice the total transconductance of the matched one, indicating a better gain performance of a mismatched interface.

A.3 Mismatched interface and simulation results

Taking the theoretical analysis mentioned above, a simple EM simulation is given to a monopole antenna designed with a receiving frequency at 73Ω using CST Microwave Studio. Figure A.3 shows the S11 parameter of the narrow band antenna. The narrowband antenna is designed for 2.4GHz application and has the minimum $|S_{11}|$ at the characteristic frequency.

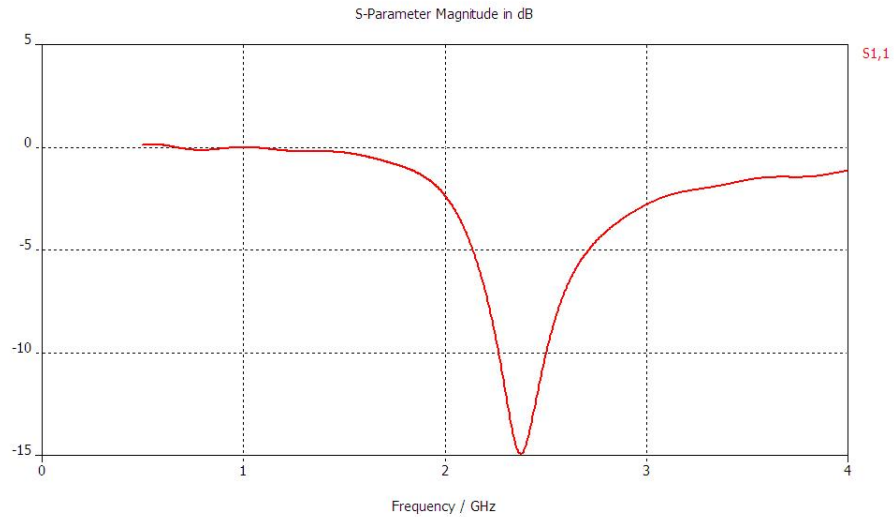


Figure A.3: $|S_{11}|$ of the ideal monopole antenna designed for 2.4GHz

Next, the antenna is changed to the receiving mode by replacing the excitation signal source with a lumped element which is a series RLC network with a resonant frequency of 2.4GHz ($\frac{1}{2\pi\sqrt{LC}} = 2.4G$), the R is used to model the equivalent resistive part created by inductive degeneration. The setup of this simulation is shown in Figure A.4. With variations on the resistor value, the voltage monitored on the capacitor is plotted in Figure A.5 for different values of R. As can be seen, the voltage swing at 2.4GHz experiences an increase when R is reduced, that is, the transistor gate-source capacitor can obtain a significantly larger voltage swing than the matched case

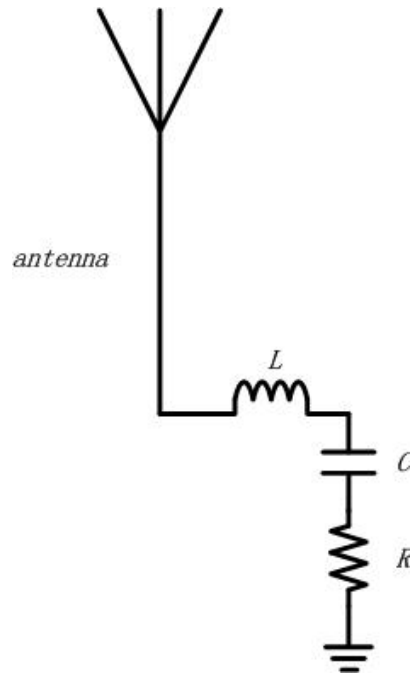


Figure A.4: Receiving mode antenna setup

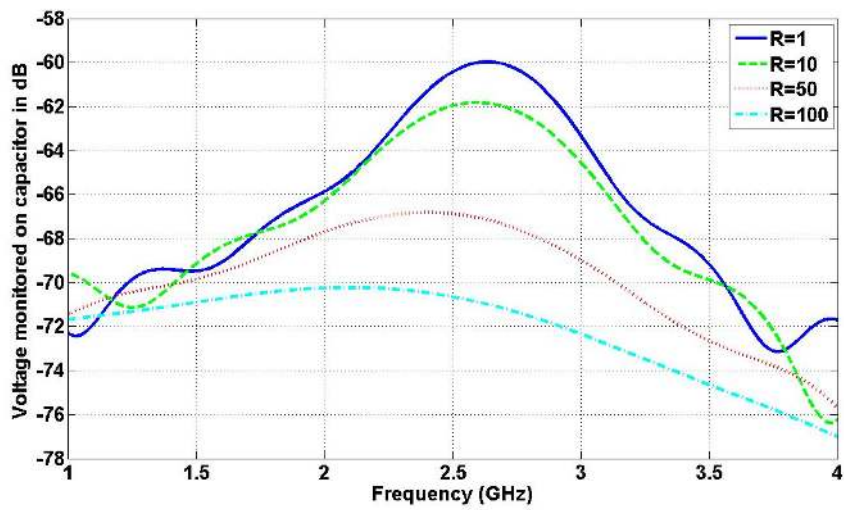


Figure A.5: Voltage monitored on the capacitor in series with a resonating inductor and a varying resistor

($R = 50\Omega$) and such an amplifier will have a larger total transconductance. Although the peak frequency is changed by a few hundred MHz, the resonating frequency can still be tuned out by the amplifier load which can be designed with a very high Q.

The worry about Inter Symbol Interference due to reflections can also be solved by connecting the antenna as close as possible to the LNA, in the best case, with no transmission line in between. In order to see the effect of inter symbol interference, a symbol with short duration time is needed for observation convenience. An ideal wideband antenna is designed with $|S_{11}| < -10$ dB in the frequency range of 4 ~ 6GHz, see Figure A.6.

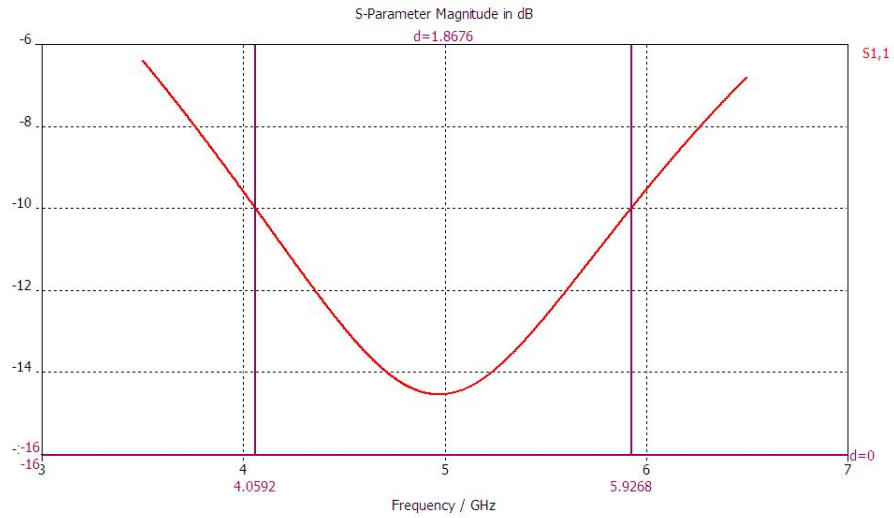


Figure A.6: $|S_{11}|$ of a wideband antenna with receiving frequency range of 4 ~ 6GHz

Using a similar setup for the receiving mode, the plane wave acting as an excitation signal of a Gaussian pulse spreading from 4-6GHz is sent to the antenna. Voltage monitored on the lumped element which is a small resistor ($R=1$), is just a delayed version of the sent signal, exhibiting no reflection effects, see Figure A.7.

Given above, we have sufficient reasoning for exploiting un-matched antenna-LNA interface property for better circuit performance.

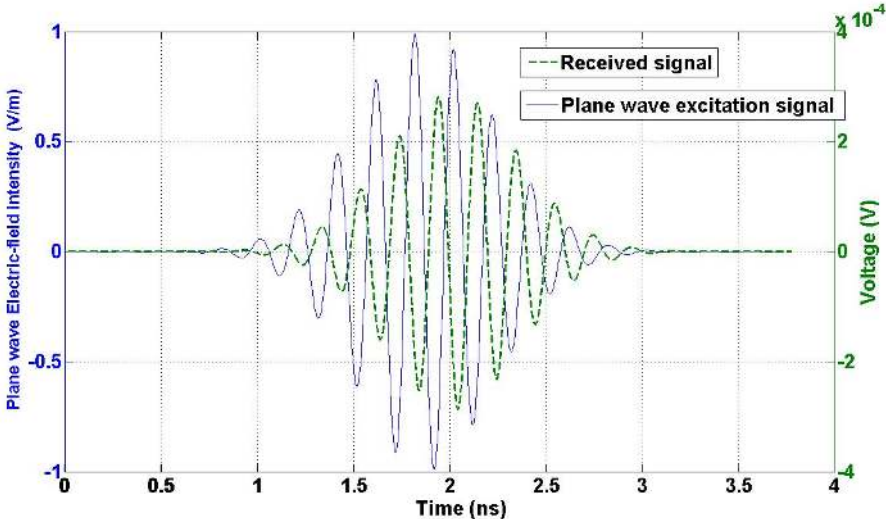


Figure A.7: Pulse received by 4 ~ 6GHz wideband antenna

Appendix B

Matlab Code

In this appendix matlab files are presented in order to increase the reproducibility of this work.

B.1 Matlab Code UWB Pulse Generator (Chapter 4)

```
% a0.control.m

soort='p' % p=pulse s=step
fe='1' % first element c, l
n=3
marginn='geen' % the sys with or without margin 'geen' 'well'
factor_sweep=0;
min.L=400e-12;

a1.system.design; % the output is sys; bode(sys)

a4.LC.values.calculation.correct;

disp('L ratio')
max(Lnew)/min(Lnew)
disp('C ratio')
max(Cnew)/min(Cnew)
```

```

% al_system_design

if not(exist('soort'))
    soort='p';
end

if not(exist('fe'))
    fe='1';
end

if not(exist('n'))
    n = 4;
end

if not(exist('marginn'))
    marginn = 'geen';
end

if marginn=='geen'
    %%%%%%%%%%%%%%%%%%%%%%%%% without margins %%%%%%%%%%%%%%%%%%%%%%%%%
    switch n
        case 1
            Rp = .011; Rs = 150;
            begg=35.8e9 ;
            endd=begg*1.0215;
            Wn = [begg endd];
            ftype = 'bandpass';
        case 2
            Rp = .37; Rs = 80;
            begg=27.5e9 ;
            endd=begg*1.742;
            Wn = [begg endd];
            ftype = 'bandpass';
        case 3
            %Rp = .36; Rs = 80;
            Rp = .36; Rs = 80;
            % begg=23.8e9 ;
            % endd=begg*2.3;
            begg=25e9 ; %25 db
            begg=29e9 ; %45 db

            endd=5.5e10; % 25 db
            endd=6.1e10; % 10 db
            endd=5.8e10; % 15 db
    end
end

```

```

        Wn = [begg endd];
        ftype = 'bandpass';
    case 4
        Rp = .36; Rs = 80;
        begg=22.1e9 ;
        endd=begg*2.67;
        Wn = [begg endd];
        ftype = 'bandpass';
    case 5
        Rp = .37; Rs = 80;
        begg=21.1e9 ;
        endd=begg*2.923;
        Wn = [begg endd];
        ftype = 'bandpass';
    end

else
    %%%%%%%%%%%%%%%%%%%%%%%%%%%%%%%%%%%%%%%%%%%%%%%%%%%%%%%%%%%%%%%%%%%%%%%%% with margins %%%%%%%%%%%%%%%%%%%%%%%%%%%%%%%%%%%%%%%%%%%%%%%%%%%%%%%%%%%%%%%%%%%%%%%%%
switch n
    case 1
        Rp = .01; Rs = 80;
        begg=35e9 ;
        endd=begg*1.0215;
        Wn = [begg endd];
        ftype = 'bandpass';
    case 2
        Rp = .37; Rs = 80;
        begg=27.5e9 ;
        endd=begg*1.742;
        Wn = [begg endd];
        ftype = 'bandpass';
    case 3
        Rp = .1; Rs = 80;
        begg=29.5e9;      % 50 db
        endd=44.5e9;      % 50 db
        Wn = [begg endd];
        ftype = 'bandpass';
    case 4
        Rp = .1; Rs = 80;
        begg=28e9 ;
        endd=begg*1.8;
        %begg=28e9 ;
        %endd=begg*1.6;
        Wn = [begg endd];
        ftype = 'bandpass';

```



```

        end
    end

    % Transfer Function design impulse response based
    [b,a] = ellip(n,Rp,Rs,Wn,ftype, 's');
    sys1=tf(b,a);
    % [a,b,c,d]=tf2ss(cell2mat(sys1.num), cell2mat(sys1.den))
    % sys1=ss(a,b,c,d)
    % bodemag(sys1)
    % grid

    [sig, time]=impulse(sys1);
    [freq, spec]=psd(sig, 1/(time(2)-time(1)), 1e4);
    plot(freq,20*log10(spec/max(spec)), 'k');
    grid
    set(gca, 'xlim', [3.1e9 10.6e9]);
    hold on

    % Transfer Function design impulse response based
    [z p]=tf2zp(cell2mat(sys1.num),cell2mat(sys1.den)) ;
    z=[z;0];
    sys2=zpk(z, p, 1);
    [sig, time]=step(sys2);
    [freq, spec]=psd(sig, 1/(time(2)-time(1)), 1e4);
    plot(freq,20*log10(spec/max(spec)), 'k-.');

    [a,b,c,d]=zp2ss(cell2mat(sys2.z), cell2mat(sys2.p),1);
    [num,den]=ss2tf(a,b,c,d);
    sys2=myorth_ladder(sys2);

    [a, b, c, d]=tf2ss(cell2mat(sys1.num), cell2mat(sys1.den));
    sys1=ss(a,b,c,d);
    sys1=myorth_ladder(sys1);

    if soort=='s'
        'type s'
        sys=sys2
    elseif soort=='p'
        'type p'
        sys=sys1
    end

    % a4_LC_values_calculation_correct

```

```

a=sys.a;
b=sys.b;
c=sys.c;
d=sys.d;

% bode(a,b,c,d)
% hold on
% m=max(abs(c))
% c=c/m
% d=d/m
% bode(a,b,c,d)

alfa=zeros(1,length(a));
for i=1:length(a)-1
    alfa(i)=abs(a(i,i+1));
end
for i=length(a)
    alfa(i)=abs(a(i,i));
end

values=zeros(size(alfa));
f=zeros(size(alfa));
i=1;
f(1)=1;
f(2)=1;
values(1)=1/alfa(1);
for i=2:length(a)-1
    values(i)=f(i-1)/f(i)/alfa(i-1);
    f(i+1)=alfa(i)*f(i)*values(i);
end
values(end)=f(end-1)/f(end)/alfa(end-1);
disp('L C values are:');
disp(values);

if soort=='p'
    R=alfa(end)*values(end);
elseif soort=='s'
    R=1/alfa(end)/values(end);
else
    disp('WRONG INPUT');
end

```

```

disp('R is:');
disp(R);
disp('c matrix new is:');
c_matrix_new=c./f;
c_matrix_new=c_matrix_new/max(abs(c_matrix_new));
disp(c_matrix_new);

% very important whether the first element is an l or a c
if soort=='p'
    L=values(2:2:end);
    C=values(1:2:end);
elseif soort=='s'
    L=values(1:2:end);
    C=values(2:2:end);
end

if fe=='c'
    C=values(1:2:end);
    L=values(2:2:end);
elseif fe=='l'
    L=values(1:2:end);
    C=values(2:2:end);
end

%
% the factor to scale the max L to 2.5e9

if factor_sweep==0
    ff=min.L/min(L);
elseif factor_sweep==1
    ff=ff;
end

%
% disp('%%%%%%%%%%%%%%%%%%%%%%%%%%%%%%%%%%%%%%%%%%%%%%%%%%%%%%%%%%%%%%%%%%%%%%%%')
% disp('%%%%%%%%% results %%%%%%%%%')
% disp('%%%%%%%%%%%%%%%%%%%%%%%%%%%%%%%%%%%%%%%%%%%%%%%%%%%%%%%%%%%%%%%%%%%%%%%%')
% disp('L :');
Lnew=L*ff;
Cnew=C/ff;
% disp('R is:');

```

```

if fe=='c'
    Rnew=R*ff;
elseif fe=='l'
    Rnew=ff/R;
end

%
% disp('c1 and c2 in f:')
%
if sum(abs(c_matrix_new(1:2:end)))>sum(abs(c_matrix_new(2:2:end)))
    vg=c_matrix_new(1:2:end);
else
    vg=c_matrix_new(2:2:end);
end

% in case the c_matrix_new = [-1 -x +y 0] the c_matrix_new has to be
% divided by 2
% vg=abs(vg/2);
vg=abs(vg);
%
% % the one component which is

vg(find(vg==max(vg)))=vg(find(vg==max(vg)))/2;

%      |
%      —
% c11—
%      |
%      |
%      —
% c12—
%      |
%      |
c1=[];
c2=[];

for i=1:length(c)/2
    c11=Cnew(i)/(1-vg(i));
    c12=Cnew(i)/vg(i);
    c1=[c1 c11];
    c2=[c2 c12];
end

%

```

```

disp('Lnew (nano), Cnew (pico), Rnew, c1, c2');
disp(Lnew*1e9)
disp(Cnew*1e12)
disp(Rnew)
disp(c1*1e12)
disp(c2*1e12)

% a5_translate_to_cadence.m

total={};
for i=1:4
    total{i}=Lnew(i);
end
length1=length(total);
for i=1:4
    total{i+length1}=Cnew(i);
end
length1=length(total);
for i=1
    total{i+length1}=Rnew(i);
end
c_matrix_new=c_matrix_new/max(abs(c_matrix_new))
length1=length(total);
for i=1:4
    if abs(c_matrix_new(1))>abs(c_matrix_new(2));
        total{i+length1}=c_matrix_new(2*i-1);
    else
        total{i+length1}=c_matrix_new(2*i);
    end
end

% add Vin
length1=length(total);
total{1+length1}=1;
variable={'L2', 'L4', 'L6', 'L8', 'c1', 'c3', 'c5', 'c7', 'r', 'g1', 'g2', 'g3', 'g4', 'Vin'};

expression=total

% a6_set_to_cadence
txt='(';
for i=1:length(variable)
    txt=[txt 'tmp' num2str(i) ' ']; %#ok<AGROW>

```

```

end
txt(end)=')';
txt=[txt '\n'];

fid=fopen(file,'w');
fprintf(fid,'savedComponent = (let\n');
fprintf(fid, txt);

for i=1:length(variable)
    fprintf(fid,['(unless tmp' num2str(i) '\n']);
    fprintf(fid,['tmp' num2str(i) ' = make_sevVariableStruct()\n']);
    fprintf(fid,')\n');
    fprintf(fid,['(unless tmp' num2str(i) '\n']);
    fprintf(fid,['tmp' num2str(i) ' = (ncons nil)\n']);
    fprintf(fid,')\n');
    fprintf(fid,['tmp' num2str(i) '->name = "' char(variable(i)) '"\n']);
    fprintf(fid,['tmp' num2str(i) '->expression = "' num2str(cell2mat(expression(i))) '"\n']);
    fprintf(fid,['tmp' num2str(i) '->index = ' num2str(i) '\n']);
end
fprintf(fid,' \n');
fprintf(fid,' \n');
fprintf(fid,['list' txt]);
fclose(fid);

```

B.2 Matlab Code Band Rejection Filter (Chapter 6)

```

soort='p' % p=pulse s=step
soort='s' % p=pulse s=step
fe='1' % first element c, 1

n=2
marginn='geen' % the sys with or witout margin 'geen' 'well'

al.system.design.band.reject; % the output is sys; bode(sys)
sys

factor_sweep=0;

min.L=400e-12;
a4.LC-values_calculation_correct;

```

```

if not(exist('soort'))
    soort='p';
end

if not(exist('fe'))
    fe='1';
end

if not(exist('n'))
    n = 4;
end

if not(exist('marginn'))
    marginn = 'geen';
end

[b,a] = ellip(n,.36, 80,[29e9 5.5e10],'stop', 's');
[b,a] = ellip(n,.36, 80,[2*pi*3e9 2*pi*10e9],'stop', 's');
p=bodeoptions;
p.FreqUnits='Hz';
% bode(b,a,p)

[a,b,c,d]=tf2ss(b,a)
sys=ss(a,b,c,d)
% bode(sys,p)

sys=myorth_ladder(sys);

```

This function is written by Michiel Grashuis a M.Sc. student in ELCA group

```

%-----
%H = myorth_ladder(TF) returns the state-space description (H) representing
%an orthonormal filter. TF is the transfer function containing the
%coeffecients in the numerator and denominator, starting with the highest
%order coefficient.
%-----

```

```
function H = myorth_ladder(sys,tf)
```

```

[num den] = tfdata(sys,tf,'v');
D=num(1);
%fill up with zeros in num

```

```

m = length(num);
n = length(den);
if (m≠n)
    num1 = num;
    for i=1:1:(n-m)
        num(i) = 0;
    end
    for i=(n-m)+1:1:n
        num(i) = num1(i-(n-m));
    end
end

%Check whether partial fraction expansion is needed
if num(1)≠0
    num=num-num(1)*den;
end;

N=length(den);
%separate odd and even denominator coefficients
if mod(N,2)==0 %returns X - n.*Y where n = floor(X./Y)
    for i=1:ceil(N/2)
        first(i)=den(2*i-1);
        second(i)=den(2*i);
    end;
else
    first(1)=den(1);
    for i=2:ceil(N/2)
        first(i)=den(2*i-1);
        second(i-1)=den(2*i-2);
    end;
end;

%loop for getting reactances
for i=1:(N-1)
    r(N-i)=first(1)/second(1);
    first=first(2:end)-r(N-i)*[second(2:end), zeros(1, (length(first(2:end))-length(second(2:end))))];
    temp=first;first=second;second=temp;
end;

%convert reactances in orthonormal coefficients
alpha(N-1)=1/r(N-1);
alpha(1:end-1)=1./sqrt((r(1:end-1).*r(2:end)));

%calculate F

```



```

beta1=sqrt(r(1)/pi);
F(1,N-1)=beta1*den(N);
F(2,N-2)=F(1,N-1)/alpha(1);
for i=3:N-1
    F(i,:)=( [F(i-1,2:end),0]+alpha(i-2)*F(i-2,:))/alpha(i-1);
end;

%create state space system
A=diag(alpha(1:end-1),1)+diag(-alpha(1:end-1),-1);
A(N-1,N-1)=-alpha(N-1);
B(N-1)=sqrt(alpha(N-1)/pi);
B=B.';
C(N-1)=num(2)/F(N-1,1);
C(N-2)=num(3)/F(N-2,2);
for i=3:N-1
    C(N-i)=(num(i+1)-C*F(:,i))/F(N-i,i);
end;

H=ss(A,B,C,D);

```

Bibliography

- [1] X. Shen, M. Guizani, R. C. Qiu, and T. Le-Ngoc. *Ultra-wideband wireless communications and networks*. John Wiley & Sons, Ltd., 2006.
- [2] J.R. Fernandes, H.B. Goncalves, L.B. Oliveira, and M.M. Silva. A pulse generator for uwb-ir based on a relaxation oscillator. *Circuits and Systems II: Express Briefs, IEEE Transactions on*, 55(3):239–243, March 2008.
- [3] S. Bagga, Z. Irahauten, S.A.P. Haddady, W.A. Serdijn, J.R. Long, and J.J. Pekarik. A uwb transformer-c orthonormal state space band-reject filter in 0.13 m cmos. *Solid-State Circuits Conference, 2008. ESSCIRC 2008. 34th European*, pages 298–301, Sept. 2008.
- [4] Shanthi Pavan. Power and area-efficient adaptive equalization at microwave frequencies. *Circuits and Systems I: Regular Papers, IEEE Transactions on*, 55(6):1412–1420, July 2008.
- [5] Marco Pausini. *Autocorrelation Receivers for Ultra Wideband Wireless Communications*. PhD thesis, TUDelft, Delft, Netherlands, December 2007.
- [6] D. Geer. Uwb standardization effort ends in controversy. *IEEE Computer Society*, 39(7):13–16, July 2006.
- [7] Airlink project. <http://www.airlink.tudelft.nl/>.
- [8] First Report and Order, FCC 02-48, Federal Communications Commission, ET Docket 98-153, February 2002.
- [9] Second Report and Order and Second Memorandum Opinion and Order, FCC 04-285, Federal Communications Commission, ET Docket 98-153, December 2004.
- [10] Robert A. Scholtz, David M. Pozar, and Won Namgoong. Ultra-wideband radio. *EURASIP J. Appl. Signal Process.*, 2005(1):252–272, 2005.

- [11] T.; Yamazato T. Jamalipour, A.; Wada. A tutorial on multiple access technologies for beyond 3g mobile networks. *Communications Magazine, IEEE*, 43(2):110–117, Feb. 2005.
- [12] J. foerster, the performance of a direct-sequence spread ultra-wideband system in the presence of multipath, narrowband interference and multiuser interference.
- [13] Robert A. Scholtz, David M. Pozar, and Won Namgoong. Ultra-wideband radio. *EURASIP J. Appl. Signal Process.*, 2005(1):252–272, 2005.
- [14] M. z. win and r. a. scholtz, ultra-wide bandwidth time-hopping spreadspectrum impulse radio for wireless multiple access communications.
- [15] S. Bagga, S.A.P. Haddad, K. van Hartingsveldt, S. Lee, W.A. Serdijn, and J.R. Long. An interference rejection filter for an ultra-wideband quadrature down-conversion autocorrelation receiver. In *Circuits and Systems, 2005. ISCAS 2005. IEEE International Symposium on*, pages 5357–5360 Vol. 6, May 2005.
- [16] N. van Stralen, A. Dentinger, II Welles, K., Jr. Gaus, R., R. Hoctor, and H. Tomlinson. Delay hopped transmitted reference experimental results. In *Ultra Wideband Systems and Technologies, 2002. Digest of Papers. 2002 IEEE Conference on*, pages 93–98, 2002.
- [17] Hyunseok Kim, Youngjoong Joo, and Sungyong Jung. A tunable cmos uwb pulse generator. *Ultra-Wideband, The 2006 IEEE 2006 International Conference on*, pages 109–112, Sept. 2006.
- [18] J.F.M. Gerrits and J.R. Farserotu. Wavelet generation circuit for uwb impulse radio applications. *Electronics Letters*, 38(25):1737–1738, Dec 2002.
- [19] Mi-Kyung Oh, Jae-Young Kim, and Kwang-Roh Park. Digitally-controlled uwb pulse generator for ieee 802.1 5.4a systems. *Consumer Electronics, 2007. ICCE 2007. Digest of Technical Papers. International Conference on*, pages 1–2, Jan. 2007.
- [20] Haolu Xie, Xin Wang, Albert Wang, Bo Qin, Hongyi Chen, Yumei Zhou, and Bin Zhao. A varying pulse width second order derivative gaussian pulse generator for uwb transceivers in cmos. *Circuits and Systems, 2007. ISCAS 2007. IEEE International Symposium on*, pages 2794–2797, May 2007.
- [21] J.M.H. Karel, R.L.M. Peeters, R.L. Westra, S.A.P. Haddad, and W.A. Serdijn. An l2-based approach for wavelet approximation. In *Decision and Control, 2005*

- and 2005 European Control Conference. CDC-ECC '05. 44th IEEE Conference on, pages 7882–7887, Dec. 2005.
- [22] D. Barras, F. Ellinger, H. Jackel, and W. Hirt. Low-power ultra-wideband wavelets generator with fast start-up circuit. *Microwave Theory and Techniques, IEEE Transactions on*, 54(5):2138–2145, May 2006.
- [23] A. Cacciatori, L. Lorenzi, and L. Colalongo. A power efficient hbt pulse generator for uwb radars. In *Circuits and Systems, 2007. ISCAS 2007. IEEE International Symposium on*, pages 3916–3919, May 2007.
- [24] S. Bagga, S.A.P. Haddad, W.A. Serdijn, and J.R. Long. An fcc compliant pulse generator for ir-uwb communications. *Circuits and Systems, 2006. ISCAS 2006. Proceedings. 2006 IEEE International Symposium on*, pages 4 pp.–, May 2006.
- [25] S.A.P. Haddad, S. Bagga, and W.A. Serdijn. Log-domain wavelet bases. *Circuits and Systems, 2004. ISCAS '04. Proceedings of the 2004 International Symposium on*, 1:I–1100–3 Vol.1, May 2004.
- [26] N. Krishnapura, V. Gupta, and N. Agrawal. Compact lowpass ladder filters using tapped coils. In *Circuits and Systems, 2009. ISCAS 2009. IEEE International Symposium on*, pages 53–56, May 2009.
- [27] Fred S Lee. *Energy Efficient Ultra-Wideband Radio Transceiver Architectures and Receiver Circuits*. PhD thesis, Massachusetts Institute of Technology, Boston, New York, 2007.
- [28] S. Wang. *Design of Ultra-Wideband RF Front-End*. PhD thesis, Stanford University, Stanford, California, 2005.